2-1-2012

Numerical analysis of a tape spring hinge folded about two axes

Bryan Estvanko

Bryan D. Estvanko
Candidate

Civil Engineering
Department

This thesis is approved, and it is acceptable in quality and form for publication:

Approved by the Thesis Committee:

Dr. Arup K. Maji, P.E. , Chairperson

Dr. Percy Ng, P.E.

Dr. Ashok K. Ghosh, P.E.

NUMERICAL ANALYSIS OF A TAPE SPRING HINGE FOLDED ABOUT TWO AXES

by

BRYAN D. ESTVANKO

BACHOLOR OF SCIENCE IN CIVIL ENGINEERING

THESIS

Submitted in Partial Fulfillment of the
Requirements for the Degree of

Master of Science

Civil Engineering

The University of New Mexico
Albuquerque, New Mexico

December, 2011

DEDICATION

To my wife and parents for their unconditional love and support in helping me to attain all of my accomplishments.

ACKNOWELGEMENTS

I would like to thank God first and foremost for blessing me with the skills and abilities to do this work.

I would also like to thank my wife for the love, support, and motivation she provided to help me reach my goals. My parents and family for all of their love, help, and support throughout my life. All of these people have made me the person that I am today and have made it possible for me to accomplish all that I have.

Finally I would like to thank my chairperson and main advisor Dr. Maji. I am thankful to have had the opportunity to work with him on this project and to have learned from him as this body of work progressed. I would also like to thank Dr. Percy for his help in learning to use Abaqus™. His guidance helped me understand how to correctly run the computer analyses. Without any of the people mentioned, this thesis would not be possible.

NUMERICAL ANALYSIS OF A TAPE SPRING HINGE FOLDED ABOUT TWO AXES

by

Bryan D. Estvanko

B.S., Civil Engineering, University of New Mexico, 2009

M.S., Civil Engineering, University of New Mexico, 2011

ABSTRACT

The ability to fold and unfold large sensor structures in space using hinges is important for space-based sensor technology. Tape spring hinges have become common in deployable space structures due to simplicity, repeatability and unique folding properties. The mechanical response of these hinges (moment-curvature, energy stored etc.) is important in ensuring safety, deployment accuracy as well as optimizing cost of the structure. In an effort to learn more about the folding and deployment properties, finite element software, Abaqus™, was used to analyze a hinge using multidirectional bending. The analysis involved large deformation (rotation through 180 degrees), nonlinear geometric loading. In order to increase confidence in the analysis procedures, a study was conducted on how the type and size of elements affects stability and buckling of a simply-supported plate. In order to fold a tape spring, a specified length of the middle segment of the hinge was first flattened, so the initial curvature about the long

axis of the hinge was removed. This minimizes the moment of inertia and hence stiffness allowing it to be folded. With the middle segment flattened, the hinge was subjected to opposite-sense bending about the hinge's short axis (axis perpendicular to the length of the tape spring). In addition to providing the needed mechanical response, the study allowed investigation into the optimum method of folding a hinge. Energy stored during folding and unfolding could be evaluated which allows the designer to determine adequate passive damping to obtain necessary post-deployment stability and pointing accuracy.

TABLE OF CONTENTS

LIST OF FIGURES

LIST OF TABLES

Chapter 1

Literature Review

1.1 Introduction to Deployable Structures

Deployable structures cover a broad range of prefabricated structures that can be transformed from a compact configuration into a larger structure of predetermined size and shape. The final deployed configuration is designed to be stable and carry loads (Gantes, 2001). Examples of terrestrial deployable structures include: emergency shelters and bridges during natural disasters; protective covers for outdoor activities, tents, umbrellas, and sailboat masts are just a few other common applications (Neogi, Douglas, & Smith, 1998). Deployable structures are a topic of ever growing interest and ongoing development.

The more common and desirable application for deployable structures is the space industry. Due to storage limitations of launch vehicles, these structures are becoming widely used in space applications. As an example, the Atlas launch vehicle has a payload capacity in a cylindrical shape of 4 m in diameter and 5 m in length (Neogi, Douglas, & Smith, 1998). This severely limits the size of structures that can be sent into space. Items such as solar panels, antennas, radars, thermal radiators, and masts are assemblies that can be folded or retracted for transportation and deployed once in space (Kiper & Soylemez, 2009). Figure 1.1 shows an example of a simple deployment of two panels.

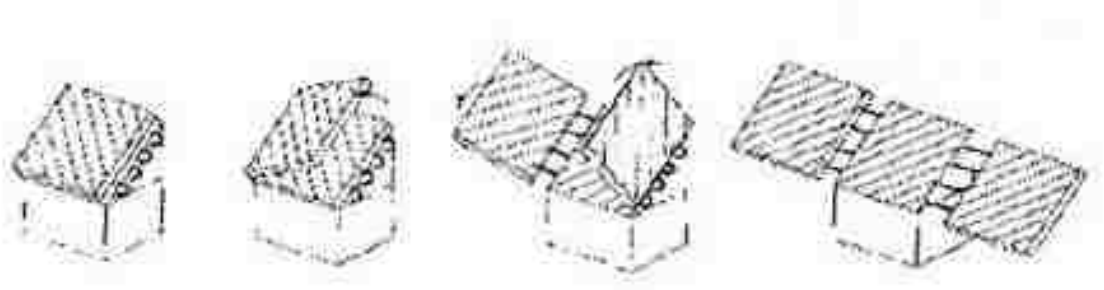

Figure 1. 1: Deployment of two panels (Seffen, Pellegrino, & Parks, 2000)

The ability to fold the structure into a compact configuration and deploy it in space has great financial advantages. Deployable structures compared to conventional structures eliminate multiple launches and the need for human assembly in space. However, this typically leads to a more complex structure due to automatic deployment mechanisms. Reliability is crucial for space applications as failure of deployment would be failure for the mission.

Deployable structures for space applications are in high demand. There are many different ways to deploy a single part or an assembly. One important aspect that is taken into consideration is the packing efficiency. Packing efficiency is the ratio of the deployed volume to the folded volume (Gantes, 2001). Typically higher packing efficiency is more economical due to maximizing the carrying capacity of the launch vehicle. Deployment can take place in one of two ways, sequentially or simultaneously. Sequential deployment involves deployment of items in various stages and tends to be more rigid during deployment. Simultaneous deployment is the deployment of all appendages at the same time (Gantes, 2001). There have been many designs that have used various methods of deployment through a variety of technologies.

1.2 Types of Deployable Structures

Deployable structures fall under two main categories, rigid assemblies and flexible assemblies. Whether the structure is rigid or flexible, the main purpose is to transform from its compact configuration to its deployed service state. Space applications of deployable structures include telescoping booms, beams for payload attachments, solar arrays, antennas, and reflectors (Neogi, Douglas, & Smith, 1998). The most common example may be a satellite that can be sent up with a number of the previously mentioned parts which are deployed to create the complete structure once in space.

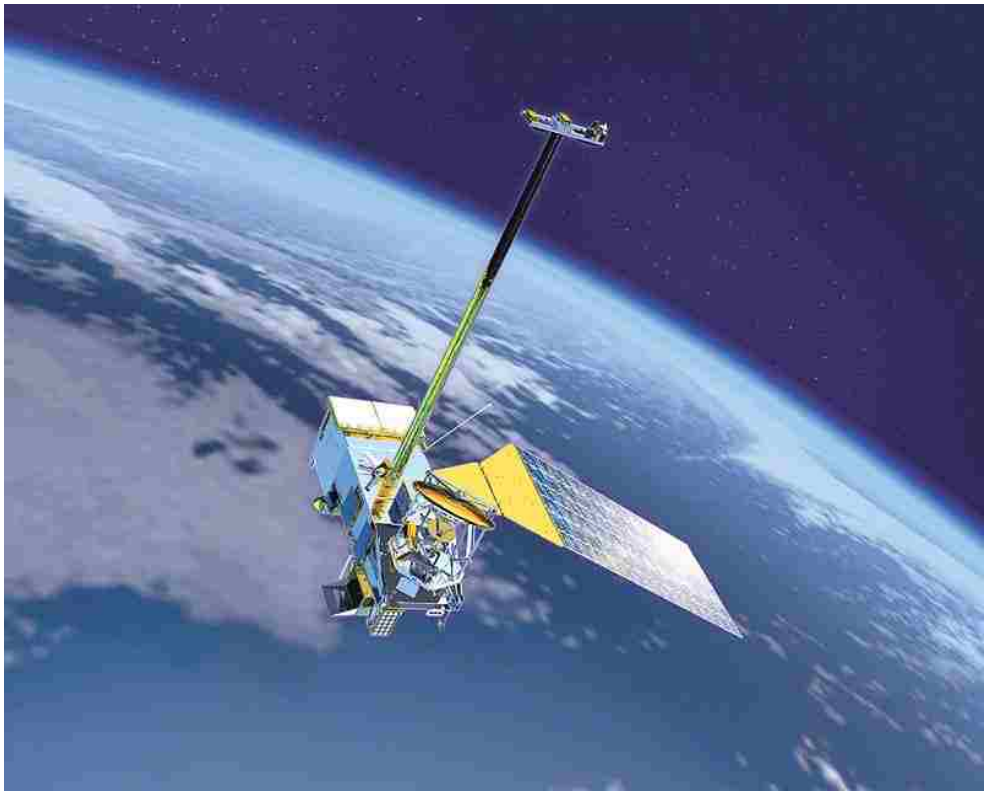

Figure 1. 2: Satellite containing various deployed assemblies (Daily, 2011)

Rigid assemblies are composed of rigid elements and joints. Typical deployments of rigid deployable structures use linkages or telescopic booms. The advantages of these systems are good shape control and a rigid structural system. This type of system may be used when precision tolerances are required or a rigid structural system is needed for vibration control. Disadvantages include complex geometric design, friction in the joints, and weight (Kiper & Soylemez, 2009).

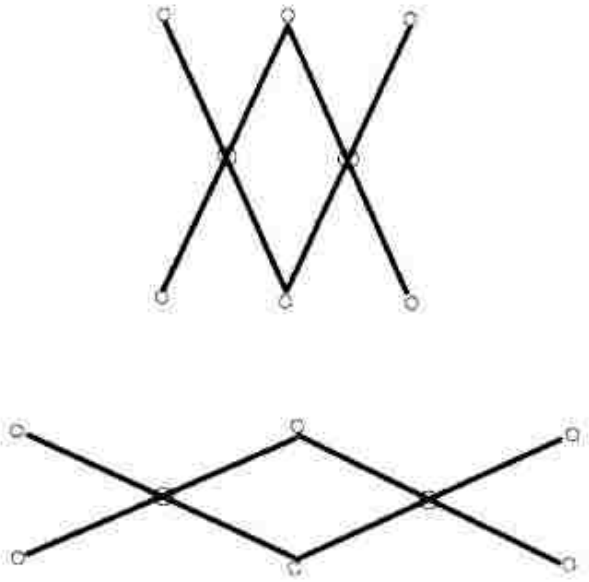

Figure 1. 3: Typical pantograph (Neogi, Douglas, & Smith, 1998)

The most common type of rigid structure is the pantograph, Figure 1.3. Once deployed the structure must be stabilized by some sort of external locking mechanism. Due to the need for a locking device, the structure is not self-supporting. A second type of rigid deployable structure is the self-supporting structure. Self-supporting structures are susceptible to buckling, reducing the load carrying capacity (Neogi, Douglas, & Smith, 1998).

Flexible assemblies may or may not include rigid elements in the whole assembly depending on the design. There are a variety of flexible assembly types of deployable structures that include but are not limited to: cable-strut assemblies, inflatable systems, and other flexible systems used to deploy parts. Cable-strut assemblies employ a system of cables and struts. The shape of the structure is dependent on the tension of the cables used to configure the linkages. Inflatable structures benefit from low stowage volume and mass, cost, and good damping properties, but lack reliability. Undesired inflation shape, stiffness, and the inability to remain inflated make these structures a difficult option (Kiper & Soylemez, 2009).

An alternative method of flexible deployment is thermally-activated members. A cable containing an internal heating element, an internal bladder, and a braided carbon-epoxy composite is flexible in its unheated state allowing for packing. Once heated by passing current through the wire, the bladder begins to inflate and provide a structural element from the cable. When the carbon-epoxy composite is heated and subsequently cooled, it cures providing permanent stiffness to the cable member. These cables can be set up in varying configurations to create numerous geometric shapes (Neogi, Douglas, & Smith, 1998).

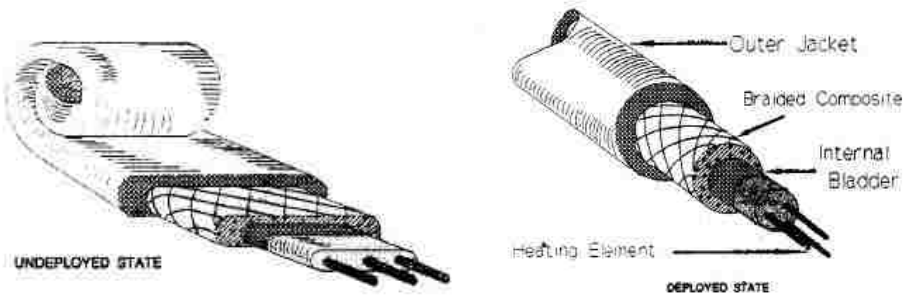

Figure 1. 4: Undeployed and deployed thermally-activated member (Neogi, Douglas, & Smith, 1998)

Deployable structures can range from very simplistic to extremely complicated. Categories include 1-D, 2-D, polygonal units for flat or curved surfaces, prismatic units, pyramidal units, etc. A member in a deployable structure should be able to withstand regular service loads and act as a deployment member without adding weight to the structure. Extra members needed for deployment or stability add expense to the structure and may require extra connections and deployment mechanisms (Gantes, 2001). Deployable space structures experience their highest failure rates during deployment (Kiper & Soylemez, 2009). A clear understanding of the components that make up the structure and proper analysis techniques greatly reduce the chance of improper deployment or structural failure.

1.3 Common Types of Hinges Used in Deployable Space Structures

There are numerous types of hinge designs used in deployable structures. The hinge type is dependent on the type of structure and the required performance parameters of the structure. Hinges can be divided into two categories, manual locking hinges and self-locking hinges.

Manual locking hinges are typically used in rigid deployable structures. This hinge requires some kind of locking mechanism to be actuated to secure the joint. To lock the joint, there is usually a mechanical device that has to be moved into place to secure the joint. This can require parts such as actuators, motors, electrical wiring, and power sources. All of these extra parts add weight and the chance for mechanical failure. Manual locking hinges are undesirable due to the need of extra components (Gantes, 2001). Friction within the deployment is a common problem with manual locking

hinges. It provides an additional force that must be overcome and causes micro-lurch during operation. Friction can also produce wear and local weaknesses leading to failure if the process is constantly repeated. These points of friction create a resisting moment or force. Lubrication can reduce the friction and wear on the parts, but introduces additional problems depending on the type of lubricant. This is common in deployable structures that use scissor like elements in their design.

Self-locking hinges are hinges that have the ability to lock once in the deployed configuration. Also known as the self-locking phenomenon, these hinge types stabilize the system once equilibrium has been reached after deployment (Hoffait, Bruls, Granville, Cugnon, & Kerschen, 2010). Self-locking hinges avoid the need for extra members, but residual stresses can lower service loads (Gantes, 2001). Many of these hinge types experience highly nonlinear behavior through the folding and deployment sequence. Self-locking hinges are found primarily in flexible assemblies due to their non rigid folding properties.

The most popular type of self-locking hinge due to its simplicity is the tape spring hinge. A tape spring (Figure 1.5), also referred to as carpenters tape, is a straight strip of material with a curved cross section (Walker & Aglietti, 2007). During deployment of an assembly, a tape spring hinge simultaneously achieves actuating, guiding, and self-locking functions all without friction elements (Hoffait, Bruls, Granville, Cugnon, & Kerschen, 2010).

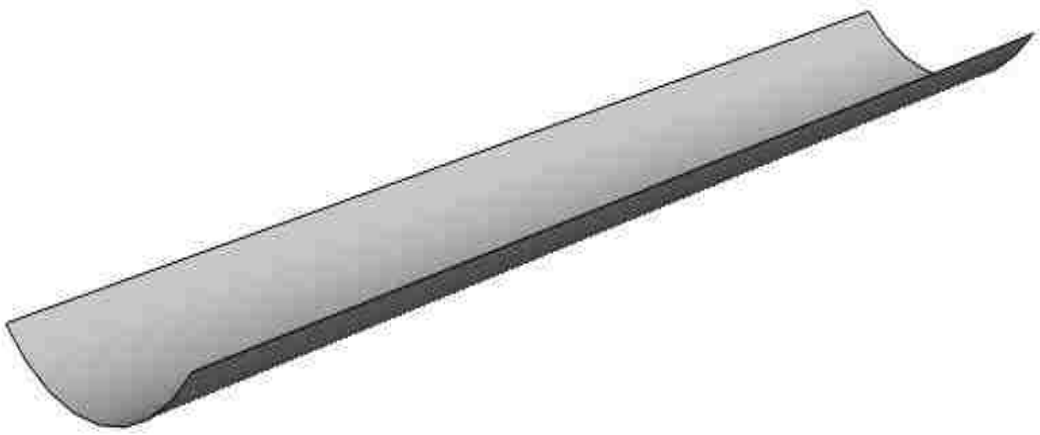

Figure 1. 5: Typical tape spring

Composite tube hinges are closely related to tape spring hinges. A tube hinge is a hinge that is constructed from a tube. The tube hinge is created by cutting two or three equally spaced slots in a thin walled composite tube (Figure 1.6). The remaining material left in the tube is essentially multiple tape springs. The composite tube hinge has the ability to be folded and retains the energy to return to its initial configuration under its own power. Tube hinges act just as tape springs, but have stronger deployment capabilities and stiffer structural properties when straight (Yee & Pellegrino, 2005).

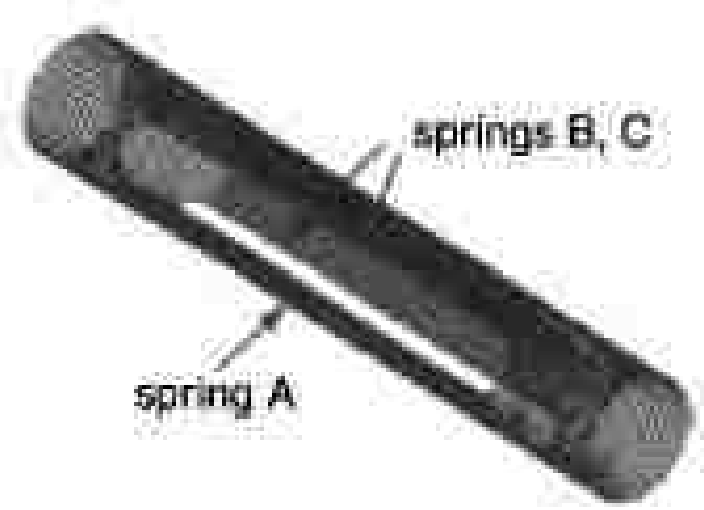

Figure 1. 6: Composite tube hinge in finite element model (Yee & Pellegrino, 2005)

Another variation of the tape spring hinge makes use of elastic memory composite materials to fold and deploy the hinge. The hinge is assembled of 'bi-lenticular' tape springs held together by aluminum clamps at both ends. Bi-lenticular configuration refers to a pair of tapes springs oriented so both concave sides face one another in a mirrored fashion. The tape springs are made of elastic memory composite laminates that have electrical resistive heaters adhesively bonded to the surface. When heated the hinge becomes workable allowing for folding to take place. The hinge is cooled once the desired degree of folding has taken place and the resin in the hinge hardens keeping the folded configuration. When deployment is desired, the heaters are turned on and the tape springs along with the elastic memory composite material return to a straight configuration. Once deployment is satisfactory, the heaters are turned off and the hinge cools and returns to a rigid state (Beavers, et al., 2002).

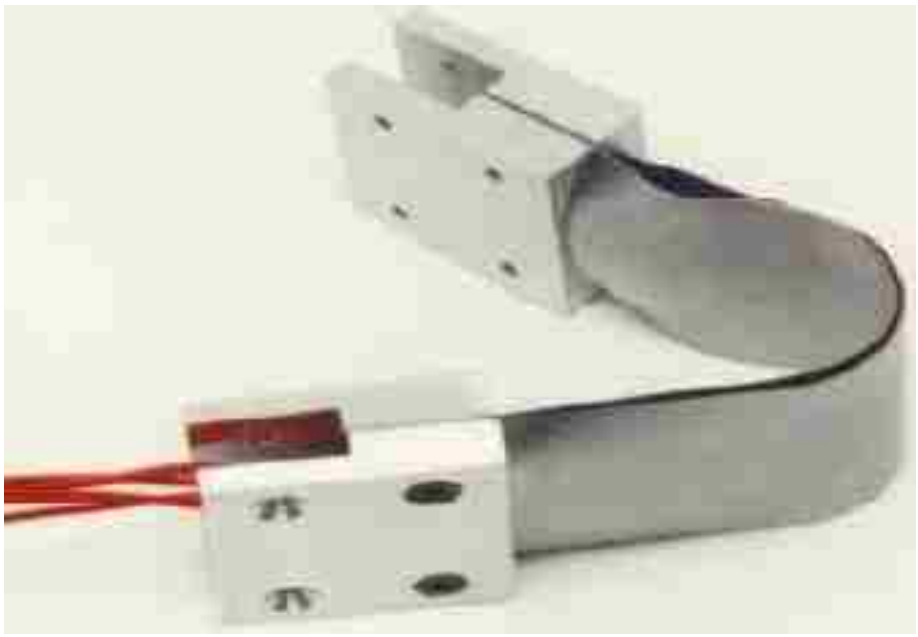

Figure 1. 7: Elastic memory composite hinge (Beavers, et al., 2002)

1.4 Tape Spring Hinges

The tape spring hinge is commonly used in deployable space structures for folding and deployment of external assemblies. Tape springs can be folded and unfolded, acting like a hinge, a deployment mechanism, a stiffener, and a locking device at a joint all simultaneously (Hoffait, Bruls, Granville, Cugnon, & Kerschen, 2010). Compared to a hinge that requires a motor or an actuator, the tape spring does not need a power source, has no internal moving parts, and has no need for lubrication (Walker & Aglietti, 2007). The minimization of parts and lack of need for a power source, make tape springs a much more reliable hinge and a lighter hinge which translates into cost savings. All of these properties provide a mechanically simple and reliable hinge design.

The curved geometry of the tape spring compared to a flat piece of material gives the tape spring greater stiffness, which helps make the structure more rigid once

deployed. In the straight configuration, the tape spring acts as a stiffener, due to its good structural properties. The straight configuration works as a locking device, because once it is straightened it is hard to get the tape spring to fold again. These properties eliminate the need for stiffeners and locking devices found in other types of hinges.

Tape springs can be folded 180 degrees in either direction and remain completely elastic. Holding torque is the maximum moment on the moment-curvature diagram. This represents the maximum moment, also called the peak moment, the tape spring can withstand. Driving torque is the residual moment after the tape spring has folded. This is the moment that is required to keep the hinge in the folded configuration, and is available for deployment (Hoffait, Bruls, Granville, Cugnon, & Kerschen, 2010).

Tape springs can be folded 180 degrees in either direction. The longitudinal folding of the tape spring so that the concave faces of the tape spring fold toward each other is known as equal-sense bending. Opposite-sense bending occurs when the tape spring is folded so the concave faces are folded away from one another (Figure 1.8).

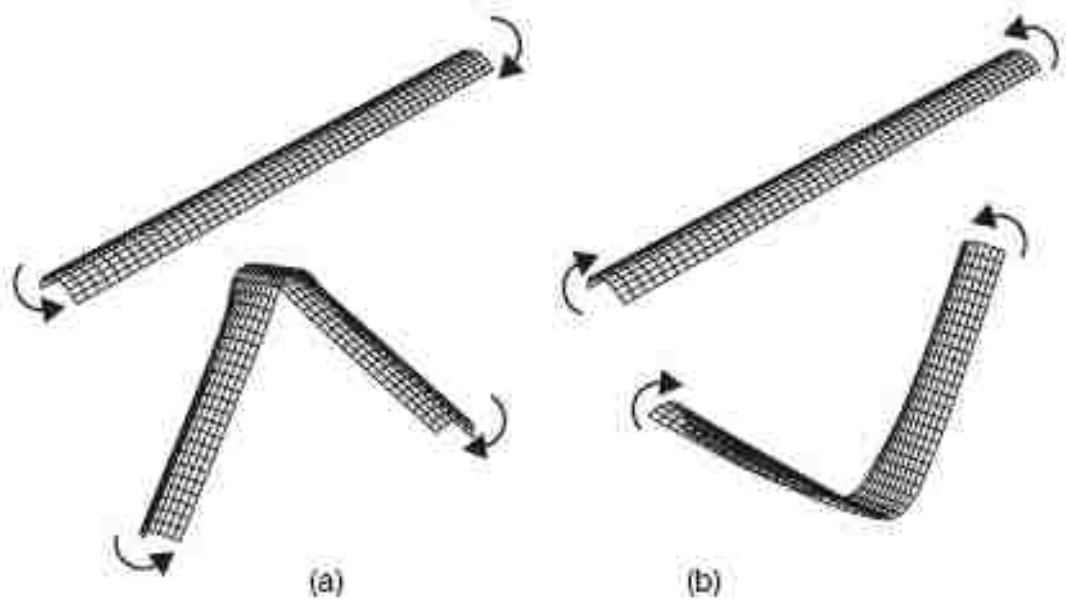

Figure 1. 8: (a) equal-sense bending (b) opposite-sense bending (Soykasap, 2007)

Opposite-sense bending produces a much greater peak moment than equal-sense bending (Soykasap, 2007). In both cases, the moment-curvature relationship is nonlinear. Figure 1.9 generalizes the moment-curvature relationship for both cases of bending.

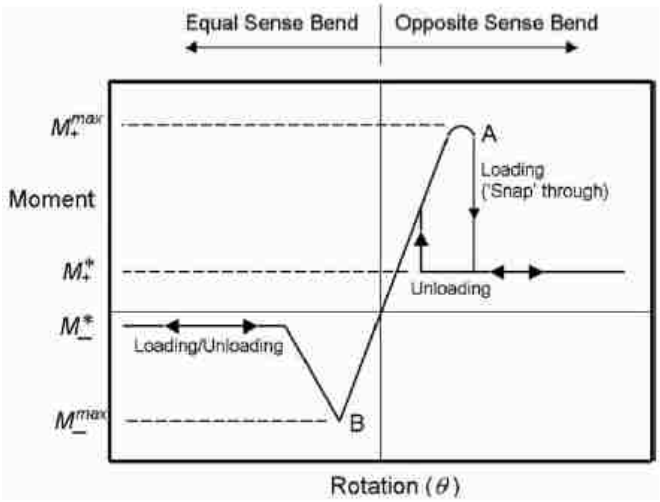

Figure 1. 9: General moment-curvature relationship (Walker & Aglietti, 2007)

Strain energy is strored when the hinge is folded. During deployment the stored strain energy is converted into kinetic energy. When the hinge straightens out the all of the energy has been released. Due to the larger peak moment of the opposite-sense bent tape spring, more energy is released compared to an equal-sense bent tape spring. To prevent the overshoot effect (oscillations before locking takes place), tape spring hinges are composed of more than one tape spring (Seffen, Pellegrino, & Parks, 2000). Two tape springs can be set next to one another facing opposite directions. Other hinges have been made up of three tape springs with two facing one direction and one facing the opposite direction as in Figure 1.10. The hinge would be folded so the single tape spring would fold in the opposite-sense direction because it creates the largest moment. When deploying, the other two tape springs help the hinge system to come to equilibrium and self-lock, by complementary opposing moments, reducing the chance of overshoot (Hoffait, Bruls, Granville, Cugnon, & Kerschen, 2010).

Figure 1. 10: Three tape spring hinge (Hoffait, Bruls, Granville, Cugnon, & Kerchen, 2010)

1.5 Finite Element Analysis of Tape Spring Hinges

Deployable structures must be designed for two completely different loading conditions: i) service loads in the deployed configuration which tend to result in small deformations and linear-elastic material response, and ii) the deployment process, during which the structure is usually subjected to geometrically nonlinear loading due to large rotations or displacements. Creating a structure to satisfy both conditions can be quite challenging. Often to accomplish a design objective an iterative design process is used as exact solutions may be very tedious and slow down the iterative process (Gantes, 2001).

Generally three failure modes are considered: strength, stiffness (related to vibration and control), and buckling (related to stiffness and strength). All three modes are considered; however one specific mode, such as stiffness, may be the most important design criteria to reduce vibrations in the structure during the service state (Gantes, 2001). The rigorous requirements and multiple failure modes make efficient designs of deployable structures challenging. The use of finite element programs help identify problem areas, make quick design changes, and reanalyze the part or structure in a timely manner.

Due to the highly nonlinear nature of the folding of tape springs, the finite element software package Abaqus™ was chosen to run analyses of tape spring hinges. Tape springs modeled by others use general-purpose shell elements also known as the S4R element (Soykasap, 2007), (Ng, 2006). To allow the program to run the analysis in a geometrically nonlinear fashion, the 'geometric nonlinear incremental analysis tool' (*NLGEOM) was applied. This tool allows the solution to be obtained through

incremental stabilization by artificial damping throughout the analysis (Yee & Pellegrino, 2005).

For the analysis of tape spring hinges it is recommended that the smallest damping factor that will still allow for convergence of the simulation be used. This damping factor is said to be $1x10^{-8}$ for many cases (Yee & Pellegrino, 2005). If the artificial damping factor is set too high, undesirable results will be obtained. One author found that a damping factor of $1x10^{-6}$ achieved the best results to match the experimental data for steel tape spring hinges (Soykasap, 2007).

In this thesis finite element analyses were conducted to determine an efficient method of folding tape spring hinges. Based upon the analytical methods of previous models, a tape spring model was constructed in Abaqus™ to test the idea of folding about two axes, which is necessary to fold and deploy a tape spring hinge. The analyses started with a model verification through the buckling analysis of a plate, a progressive approach to learn about large nonlinear bending of a plate. Subsequent analyses included determination of energy stored and moment-curvature relationships from folding and deploying (unfolding) of a tape spring about two axes.

Chapter 2

Model Verification and Large Deformation Bending

2.1 Model Validation on Buckling Analysis of a Simple Plate

When creating a finite element model (FEM) to solve a problem it is important to verify that the results are what would be expected through conventional calculations. This section will describe the process of model verification for buckling analysis of a simple aluminum plate. An arbitrary plate size was selected and the buckling load was calculated through standard equations. The plate was modeled in Abaqus™, a finite element software program, using three different model types. The analysis was validated by comparing the buckling load results from the models and the analytical solution.

An aluminum plate was modeled using arbitrary dimensions of 40 inches high by 10 inches wide by 0.25 inches thick. The modulus of elasticity, E, used was 10,000 ksi with a Poisson's ratio, ν, of 0.33. The analytical solution was found using the standard buckling load equation for columns as seen in Equation 1.

$$Pcr = \frac{\pi^2 EI}{(KL)^2} \qquad \textbf{(Eqn. 1)}$$

Where,

$$Pcr = \frac{\pi^2 (10{,}000{,}000\,psi)(0.01302 inch^4)}{(1*40 inch)^2} = 803.1 lbs \qquad \textbf{(Eqn. 2)}$$

For this equation K is dependent on the constraints of the plate at each end. In the analysis, the base of the plate is fixed from displacement in the X- and Y-direction. The top constraint is a 'roller' that resists displacement in the X-direction but allows displacement in the Y-direction. For a plate with hinged-hinged boundary condition at the

two ends, the Effective Length Factor (K) is 1 (Hibbeler, 2008). The calculated bucking load is 803.1 pounds (Eqn 2). This value was used to compare the results of the finite element buckling analysis models.

The first model created was a two dimensional deformable wire model. This type of model is shown in 2-D but can have 3-D geometry applied to it. The length of the model was first described (40 inches). Next the material properties and cross section of the plate were created (10 inches by 0.25 inches). The cross sectional and material properties were applied to the whole 40 inch long 2-D wire. Although the model looks to be a simple wire, as seen in Figure 2.1, it is actually modeling a 3-D object. The same constraints were applied to this model as previously described.

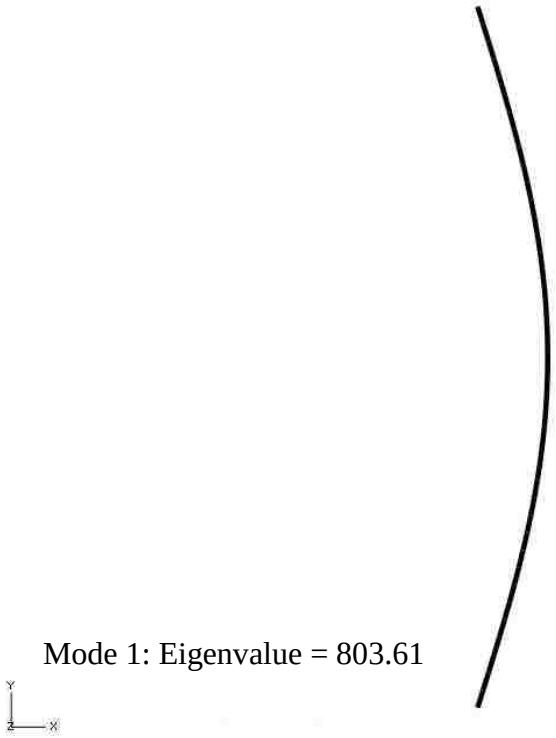

Figure 2. 1: 2-D wire model deformed shape mode shape 1

After the model was created the bucking analysis was run. Abaqus™ uses the mode shapes of the deformed object and calculates the Eigenvalues corresponding to the

mode shapes. Typically, in space structures design the fundamental frequency that corresponds to the first mode is of interest. The bucking load is equal to the load applied multiplied by the Eigenvalue. Simply applying a load of one pound results in the Eigenvalue being equal to the bucking load. The buckling load for the deformable wire model was 803.61 pounds; very close to the analytically calculated buckling load (803.1 pounds); the negligible difference of 0.06 percent verified that the calculated solution and the modeled solution are acceptable.

The next model created was a 3-D solid element model of the plate with the same material properties and dimensions as the previous cases. To apply the same constraints, the base was fixed from displacement in the X-, Y-, and Z-directions and a roller was again applied to the top of the plate restricting motion only along the long edge of the top of the plate. Once again, a load of one pound was applied to the top of the plate.

For this analysis a mesh must be generated to calculate the buckling load. The mesh size is input by the user. In this case the dimensional units for the mesh were in inches, so a mesh size of one generates a grid of nodes and elements that are spaced at one inch intervals. The type of element used in this analysis was a C3D8R, which is a 8-node linear brick, reduced integration, hourglass control element. This is the default element type for this mesh.

A mesh size of 2 was selected for creating the nodes needed for the analysis, see Figure 2.2. The bucking load from the analysis was 669.72 pounds, an error of 16.6 percent compared to the theoretical calculation. A convergence study with progressive mesh refinement was conducted.

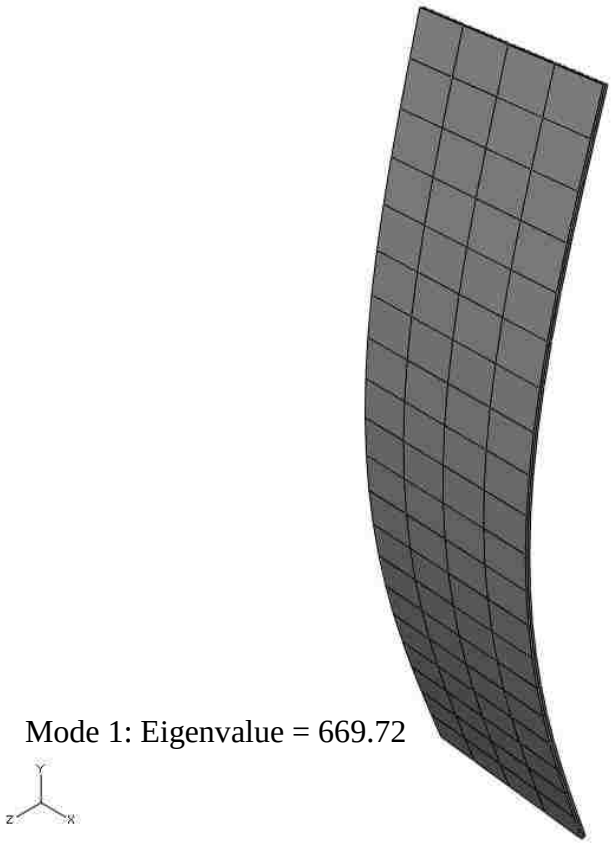

Figure 2. 2: 3-D plate model mesh size 2 mode shape 1

Table 1 shows the effect of different mesh sizes that were tried, the resulting buckling load, and percent difference compared to the previous buckling load. When using finite elements, typically a smaller mesh size, generating more elements, will yield better results. As the mesh size decreased the buckling load decreased as well, but the percent error increased. As seen in Table 1, the lower mesh sizes produced a result that converges around 609 pounds. The mesh size of 0.20 was the smallest mesh size the computer could run before running out of memory. While the solution converges at the higher number of elements, the error is about 24 percent compared to the analytical solution (803.1 pounds).

Table 1: Mesh size, buckling load, and percent difference for solid elements

Mesh Size	Buckling Load (lbs)	Percent Difference
2	669.72	-
1	633.81	5.5 %
0.50	611.90	3.5 %
0.25	609.46	0.4 %
0.20	609.33	0.02 %

It can be observed that mesh refinement reduces the buckling load due to the added flexibility. It is presumed that the lower buckling load from the 3-D analysis is also a consequence of the added flexibility and movement in 3-D (from Poisson's effect) as opposed to the restricted movement and added stiffness in the 2-D model. Figure 2.3 shows the deformed shape of the plate in its first mode shape using the mesh size of 0.20.

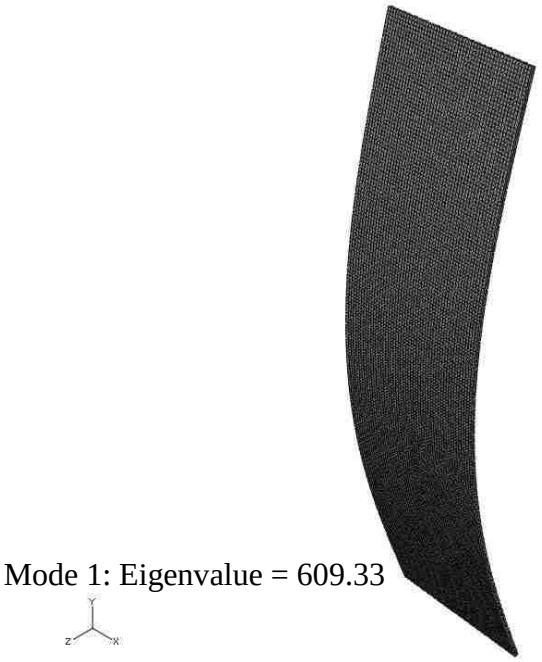

Figure 2. 3: 3-D plate model mesh size 0.2 mode shape 1

The last model created was a 3-D shell element model. This model used the same dimensions and material properties as the previous models. The same constraints were applied to the base, fixed from displacement in the X-, Y-, and Z-directions, and a roller was again applied to the top of the plate restricting motion only along the long edge of the top of the plate. Once again, a load of one pound was applied to the top of the plate.

This model also required a mesh size to run the analysis. Various mesh sizes were applied to the model to create another convergence study. Table 2 shows a convergence of the buckling load near 809 pounds. It is evident that the shell element 3-D model better simulates the buckling of the plate compared to the solid element 3-D model.

Table 2: Mesh size, buckling load, and percent difference for shell elements

Mesh Size	Buckling Load (lb)	Percent Difference
4	821.48	
2	812.58	1.08%
1	810.11	0.30%
0.5	809.45	0.08%
0.25	809.24	0.03%

As a result of the buckling analysis study two key lessons were learned. The analytical calculation gave a buckling load of 803.1 pounds. The 2-D wire model gave a bucking load of 803.6 pounds and the 3-D shell element model gave a buckling load of 809.2 pounds. These three different analyses gave a reasonably close result when solving the same problem. The 3-D solid element model gave a buckling load of 609.3 pounds, which is not within a reasonable range of the other results. This shows that using the proper element type is crucial when running a finite element model. The results of this

buckling analysis showed that the finite element software could be properly used to create other finite element models with confidence in the results.

2.2 Energy Storage During Large Deformation/Rotation of a Plate

The purpose of doing the buckling analysis accomplished three goals. The first was to get familiar with the software that is being used for this project. Next, the buckling analysis allowed the computer output to be compared to a known analytical solution. The primary goal was to analyze the large deformation folding of thin materials. Since a rotation of up to 180 degrees is the desired outcome for complete stowage (folding), the problem becomes nonlinear as the plate begins to have large deformations. Hence a nonlinear finite element program must be used to evaluate the conditions of bending the plate. Using Abaqus™ allows for many ways to approach the problem. With the inputs known, after the model has run successfully, the user can then obtain output data from the model. This output data can be anything from stresses and displacements to internal energy values.

Accurate determination of stored energy is an important parameter for safety and accurate deployment. To increase confidence in the determination of stored energy during nonlinear deformation, a plate folding model was run. The model used all of the same dimensions and material properties as in the buckling analysis. The base was fixed from displacement in all directions and the top of the plate was bounded by a roller so that it was free to move in the vertical direction but not the horizontal direction. A load case with a single point load was applied to the top center of the plate.

2.3 A Two Step Approach to Fold the Plate

To get the plate to fold through the full 180 degrees, a unique method was applied. This method consisted of loading the plate in two steps. The first step applied a very small horizontal load at the midpoint of the plate to generate a slight bow in the plate. This small deformation of the plate would help the plate to bend because it would no longer be a straight member. The second step would apply the vertical load at the top of the plate. Figure 2.4 shows an example of the two step loading process

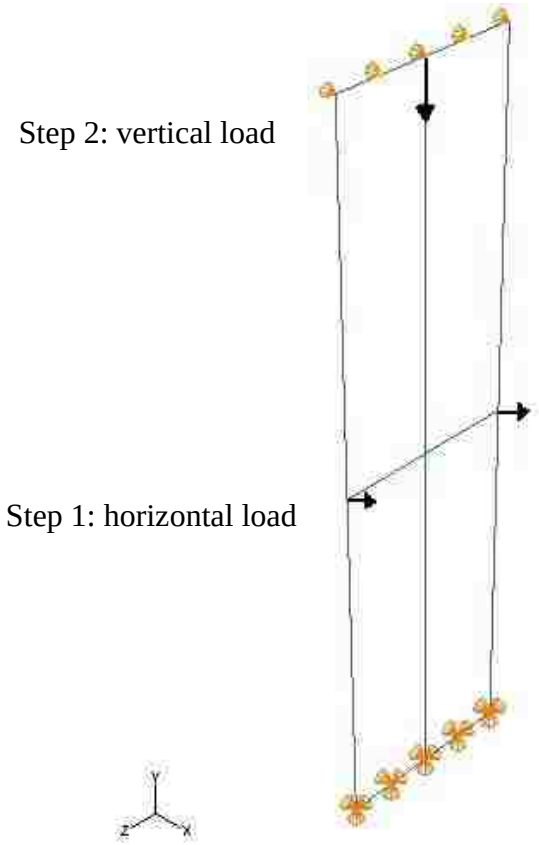

Figure 2. 4: Two Step loading process: arrows indicate point loads and 'fans' indicate boundary conditions

Using the two step method allows the plate to bend because the member is no longer perfectly straight. If the member stayed perfectly straight and the applied load was exactly vertical, the plate would only compress even if the load was well beyond the buckling capacity due the exact nature of the analysis program.

When there are multiple loadings, as with this method, the loads can be controlled by the 'step' command in Abaqus™. The horizontal load was applied in the first step and the vertical load was applied in the second step. The user has the option to either continue to run the first step while the second step is run, or the first step can be inactivated at the beginning of the second step. For this case the first step was inactivated once the second step was begun. The purpose of the first step is to create a slight imperfection in the member before the vertical load is applied. Continuing the horizontal force while loading the plate vertically would not represent the problem being modeled.

Another modification was made to the model to help produce larger deformations to the plate. This was the use of the 'nonlinear geometry tool' found within the 'Edit Step' dialogue box. When the 'nonlinear geometry tool' is on, Abaqus™ accounts for any geometric nonlinearity during the course of the step. This feature allowed the plate to bend in a nonlinear fashion as will be shown later.

To help the program run better and capture the deformation more precisely, the 'step incrementation' was changed. This parameter helps reduce errors when analyzing the part. The increment size was changed from the default of 0.1 to 0.01. Smaller increments, or time steps, help the program produce results when running the 'nonlinear geometry tool'. While a smaller time step increases the total time for the job to run, a large time step may be too large and produce an error in the analysis.

The new plate model included the modifications previously mentioned. The plate still had the same dimensions, 40 inches tall by 10 inches wide by 0.25 inches thick. It had the same material properties of aluminum, 10,000 ksi and a Poisson's ratio of 0.33. The material is considered to be linear elastic and yielding was not taken into account for the analysis. The plate was pinned in all directions at the bottom and had a roller at the top face of the plate to restrain movement in the Z-direction. The horizontal load of one pound was applied at the middle of the plate, one on each edge as shown in Figure 2.4.

The load followed 'the global coordinate system' in order to keep the applied load in the Y-direction. This is an important detail as the loads can be set to follow the 'nodal rotation' throughout the simulation. The results of the plate bending test are discussed in the following section.

2.4 Determination of Moment-Curvature Relationship

The outcome of the plate folding model was to produce a moment-curvature graph. In order to do that, the output data had to be obtained and analyzed. To obtain the moment due to the force, the internal energy values would be used to calculate the moment values. This seemed to be the easiest way to calculate the moment because the internal energy is a default output value for all models in Abaqus™. The second reason was through much trial and error, a method of directly applying a moment to the plate yielded no results.

To determine if the energy could be accurately calculated from the FEM analyses, a simple energy problem was modeled to see if the Abaqus™ results would match the calculated energy. The problem considered was an arbitrary simple beam with

dimensions of 2 inches tall by 2 inches wide by 48 inches long. The beam was simply supported with a pin on one end and a roller on the opposite end. The material properties were taken as the same aluminum properties as previously discussed and there was a point load of 200 pound applied directly at the center of the beam.

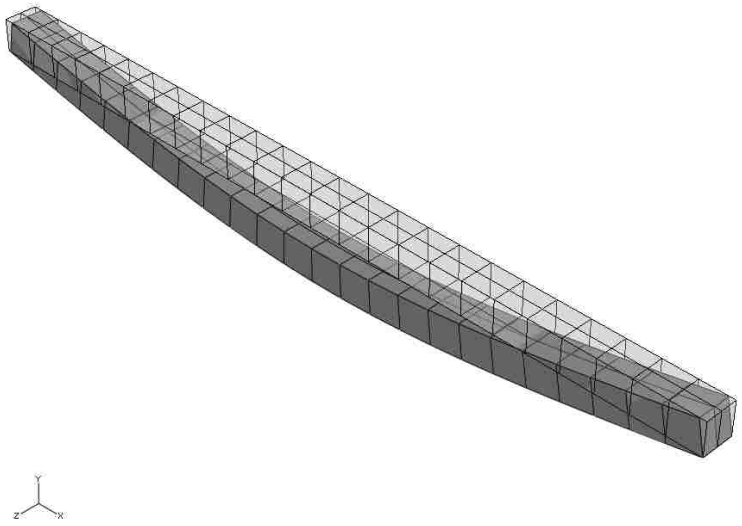

Figure 2. 5: Undeformed and deformed shape of the simple beam model

The simply supported beam model can be seen above in Figure 2.5. The vertical deflection at the center of the beam was 3.24 inches. The 'internal energy' of the beam given by Abaqus™ was 323.5 inch-pounds. Using the value of the deflection and Equation 3, the energy of the beam was calculated to compare the results.

$$Energy = \frac{1}{2} * \Delta Y * P \qquad \textbf{(Eqn. 3)}$$

Where,

ΔY = maximum deflection, inches

P = applied load, pounds

$$Energy = \frac{1}{2} * 3.24 * 200 = 324 in * lb \qquad \textbf{(Eqn. 4)}$$

Comparing the two results it is easy to see that the calculated solution, 324 inch-pounds, matches almost exactly to the value produced by Abaqus™, 323.5 inch-pounds. This simple comparison gave confidence to move forward using the internal energy values that Abaqus™ calculates.

The next step in the process was to apply this method to the plate model that has been developed throughout this paper. Once again the same aluminum plate was used with the same dimensions and boundary conditions, and the two step method was used. The first step remained the same, loading the plate horizontally at the midpoint with a one pound load at each of the two edges. The load case, a point load at the top of the center of the plate, was applied.

Table 3, shown on the next page, displays the results of a number of different magnitude loads applied to the plate. The first column in the table shows the magnitude of the load that was applied to the plate. Notice that the loading starts at 775 pounds and increases by increments of 25 pounds. At 950 pounds the plate begins to show significant deformation. Some values increased by more than 25 pounds. Not every load produced a vertical displacement, due to numerical errors experienced while running the analysis. The range of values is still good enough to get a representation of the relationship between loading and the rotation of the plate.

The second column gives the vertical displacement of the top of the plate. This displacement was used to calculate the angle of rotation of the plate. The column labeled Abaqus™ energy is the internal energy of the plate that was calculated by Abaqus™.

Table 3: Results due to a veritcal point load on the plate

Load (lbs)	Vertical Displacement (in)	Abaqus™ Energy (in-lb)	Θ (deg)	Moment (in-lb)
0	0	0	0	0
750	0.002	1.1	0.0	177
800	0.003	1.2	0.0	177
850	0.003	1.3	0.0	177
900	0.003	1.5	0.0	177
950	5.8	5,306	26.1	205
1050	12.4	11,851	55.8	238
1150	18.0	18,007	81.0	265
1200	21.2	21,742	95.4	281
1250	22.3	23,171	100.4	286
1500	30.6	34,578	137.7	326
1550	32.0	36,606	144.0	333
1600	33.2	38,526	149.4	339
1650	34.4	40,443	154.8	345
1700	35.4	42,251	159.3	350
1725	36.0	43,139	162.0	353
1730	36.1	43,318	162.5	353

The column labeled moment shows the calculated moment based on the amount of bending that was experienced. Due to the plate's highly nonlinear deformation, the equation to calculate the moment takes into account the plastic region of the moment-curvature relationship. The moment was calculated based on Equation 5.

$$Energy = M(\theta_2 - \theta_1) \qquad \textbf{(Eqn. 5)}$$

Where,

M = moment, inch-pounds

θ = rotation, radians

Simplifying Equation 5 and solving for the moment,

$$M = \frac{dE}{d\theta} \qquad \textbf{(Eqn. 6)}$$

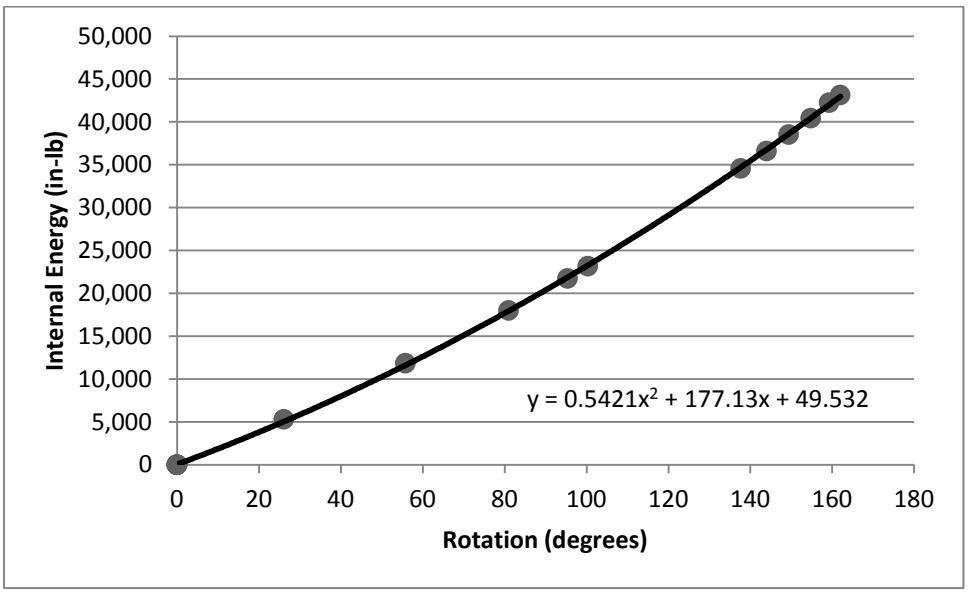

Figure 2. 6: Internal energy as a function of rotation

The Internal Energy vs. Rotation data (Figure 2.6) was plotted from Table 2. A polynomial trendline was fit to the data along with the line's equation to help solve

Equation 6. To solve for the moment, Equation 6 was diferentiated resulting in Equation 7. Equation 7 provides the moment as a function of rotation and is plotted in Figure 2.7.

$$M = 1.0842\theta + 177.13 \qquad \textbf{(Eqn. 7)}$$

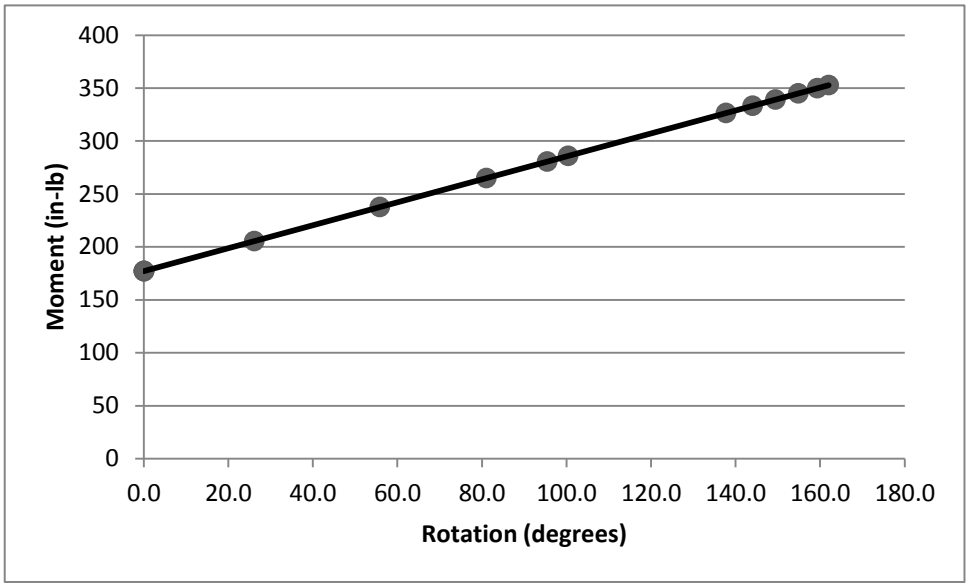

Figure 2. 7: Moment as a function of rotation

Finally, Figure 2.8 shows the plate at its maximum rotation. The maximum rotation was 162.5 degrees due to a point load of 1,730 pounds. Beyond that load the plate became unstable. It can be seen in Table 3 that the values of internal energy are close to and somewhat smaller than the product of the applied load and the resulting displacement. This is consistent with what is expected in the post-buckling nonlinear regime of this analysis.

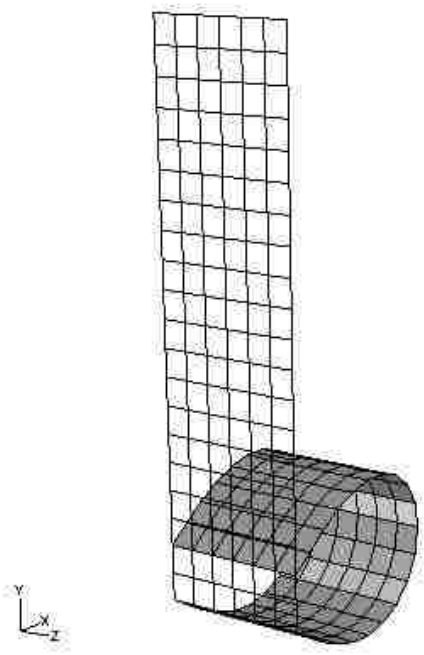

Figure 2. 8: 1,730 pound point load produced 162.5 degrees of rotation

In summation, there were a number of tasks associated with these models and many of them were accomplished. To begin, it was shown with the buckling analysis that a buckling load for a plate could be found using Abaqus™ and verified by traditional buckling equations. It was also found that the shell element gave a more accurate result than the solid element for this plate. The next goal was to try to fold a plate through significant geometrically nonlinear deformation. The task to compare internal energy outputs to load-deformation and moment-curvature relationship was accomplished. The internal energy method required the use of the tools of Abaqus™, some equation manipulation, and finally a review of the results. In all of these analyses, the project progress and the knowledge of the program increased. These flat plate models helped guide the progression of this project into the next phase.

Chapter 3

Two Axis Folding of a Tape Spring Hinge

3.1 An Optimum Method of Folding a Tape Spring Hinge

This study looks into the most efficient method of folding tape spring hinges in an effort to minimize the moment (or force) and stored energy. Rather than simply folding a tape spring by applying moments at both ends and folding about the short axis, this study investigates the effects of folding about two axes. By first flattening a middle segment of the tape spring (folding about the long axis, axis of rotation and moment being along the length of the tape spring), the moment of inertia of the cross section is lowered. Subsequent folding about the short axis (typical folding of a tape spring with the axis of rotation being perpendicular to the length of the tape spring), requires significantly less applied moment due to the flattened cross section. It also minimizes potential for damaging the material from large stresses.

This analysis was run when folding the tape spring in the opposite-sense direction. Opposite-sense folding requires a greater peak moment, Figure 1.9, than equal-sense folding. In an effort to reduce the greatest peak moment required to fold the tape spring, only the case of opposite-sense folding was studied.

3.2 Properties of Tape Spring Hinges

The dimensions of a tape spring were the same as that used by Soykasap (2007). There are four dimensions and two material properties needed to model a tape spring. These dimensions include; the thickness of the material, t, the arch length that is specified

by the angle, α, multiplied by the radius, R, and last, the length of the tape spring, L. Figure 3.1 gives a visual reference to these parameters. Since only geometric nonlinearities are of interest and to prevent damage, the material is to be kept in the elastic domain, the two material properties required are the Young's modulus, E, and the Poisson's ratio, ν.

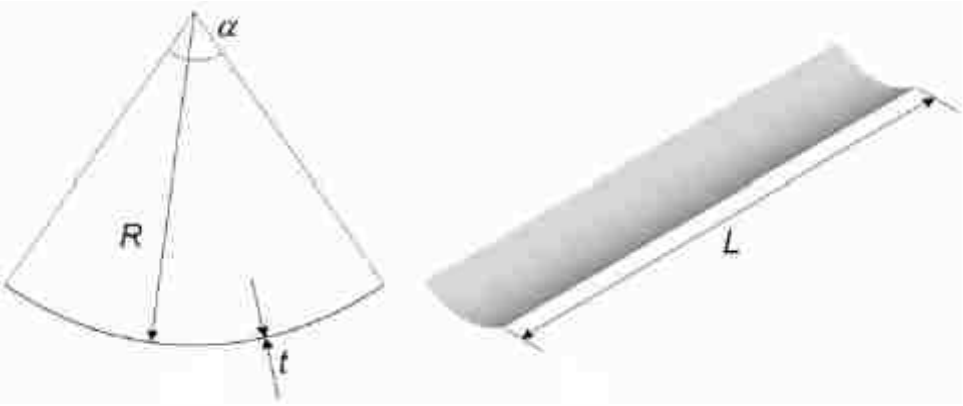

Figure 3. 1: Tape spring parameters (Aglietti, 2007)

Tape spring hinges can be made from a number of different materials. The most common materials used are typically steel or a composite material. When made from a composite material, the direction of the fibers have an effect on the behavior of the moment-curvature relationship, Figure 3.2. Different fiber oreintations with respect to the X- and Y-axis have been studied such as 0°, 90°; ±45°; 0°, ±60° (J.C.H. Yee, 2004). Due to the nature of the tape spring, the material stays in the linear elastic range throughout the bending process. This is true for both 180 degree folding in the equal and opposite-sense directions.

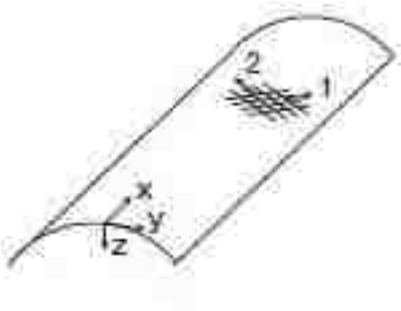

Figure 3. 2: Fiber directions in composite material tape spring (J.C.H. Yee, 2004)

3.3 Deployment of a Tape Spring Using Abaqus™

The dimensions and material properties used to model the tape spring were the following:

t = 0.115 mm
α = 86.55°
R = 16.91 mm
L = 140 mm
E = 210 Gpa
ν = 0.30

Soykasap's paper obtains data using lab experiments and Abaqus™ modeling to compare the results. The peculiar dimensions reflect that of an actual tape spring. Their paper outlines some of the parameters used in Abaqus™ to get the most accurate results to match the experiments run in the lab and helped to set up the tape spring model that would be created for this project.

Reading literature about how to model the tape spring lead to a new method to gather the results needed for the analysis of the tape spring. The model was created using shell elements rather than solid elements. Shell elements are generally used when the thickness is small compared to the other dimensions. The tape spring was created using

the default SR4, 4-node doubly curved shell element. This was the element type most commonly used by others that modeled tape springs in the literature.

A new feature that was used for the tape spring model was reference points. In Abaqus™, a reference point is a point that can be added to the model where boundary conditions can be applied. Two reference points RP-1 and RP-2 were added to the model as seen in Figure 3.3.

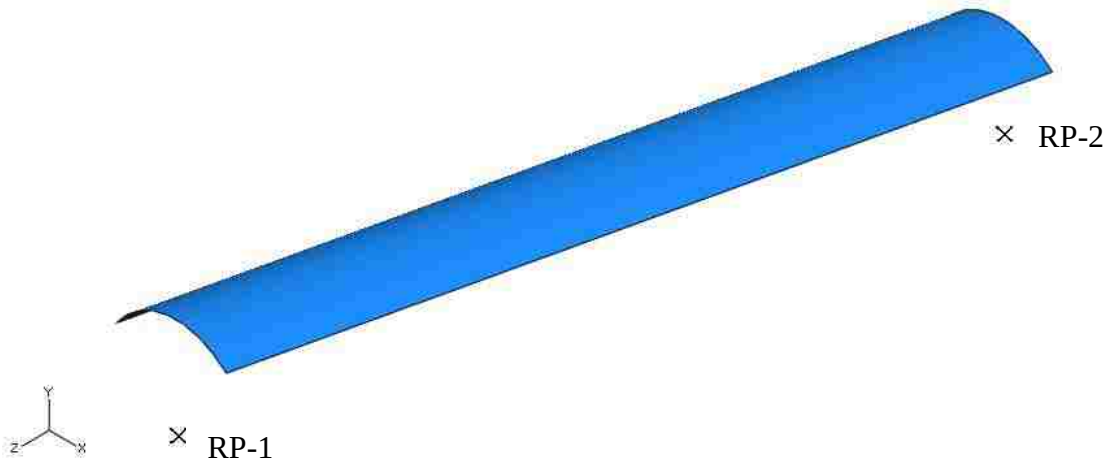

Figure 3. 3: Location of reference points

The location of the reference points is at the centroid of the arc at both ends of the tape spring. The boundary conditions were then applied to the reference points. Reference point one was set to have zero displacement in the X-, Y-, and Z-directions, and was set to have zero rotation about the Y- and Z-axes. The rotation about the X-axis was set to rotate by a specified amount of radians. Reference point two was set to have zero rotation about the Y- and Z-axes while the X-component of rotation was also specified. Reference point two was set to zero displacement in the X- and Y-directions, but the Z-direction was free to move to allow for the bending to take place.

The reference points needed to be connected to the model in order for the boundary conditions to apply to the tape spring. This was accomplished through the 'constraints' command. A 'rigid body constraint' was selected. The constraints were applied through the 'tie nodes' option. The end arc of the tape spring was selected to be the rigid body, and through the 'tie nodes' option all of the nodes along the arc were tied together and held rigid. The associated reference points were then selected to be applied to this constraint. Using this constraint keeps the two ends of the tape spring rigid throughout the bending of the tape spring as if they were clamped into the structure. The reference points act as a place to grip the model and apply a specified rotation.

The last modification that differs from the plate models is in the 'nonlinear geometry tool'. In the 'nonlinear geometry selection box', there is an option to set a 'stabilization parameter'. For the tape spring, setting the 'automatic stabilization parameter' to a specified damping factor was chosen. When Abaqus™ is solving the nonlinear problem, it introduces artificial damping to help with stabilization of the model. If the damping factor is specified, the model will give results that match more closely with experimental data (Soykasap, 2007). Many have found through trial and error that this specified damping factor should be set somewhere between 1×10^{-6} and 1×10^{-8}. For a steel tape spring 1×10^{-6} has shown accurate results when compared to experimental data. For this simulation, using steel as the material, the artificial damping factor of 1×10^{-6} was applied.

The tape spring model was completely folded, 180 degrees, in the equal-sense and opposite-sense directions. This showed that the model was working correctly and that the deformed shapes matched those seen in other models. These results are displayed in

Figures 3.4 and 3.5. Notice in both figures the ends of the tape spring have the same cross sectional arc due to the fact that they were set to be rigid.

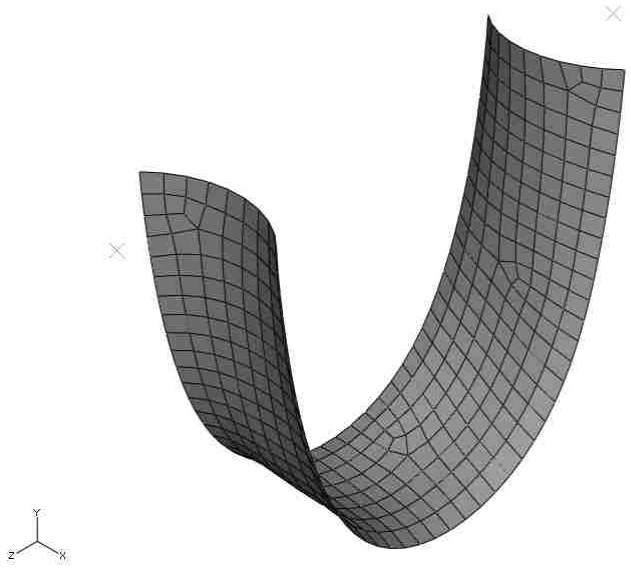

Figure 3. 4: Complete opposite-sense folding

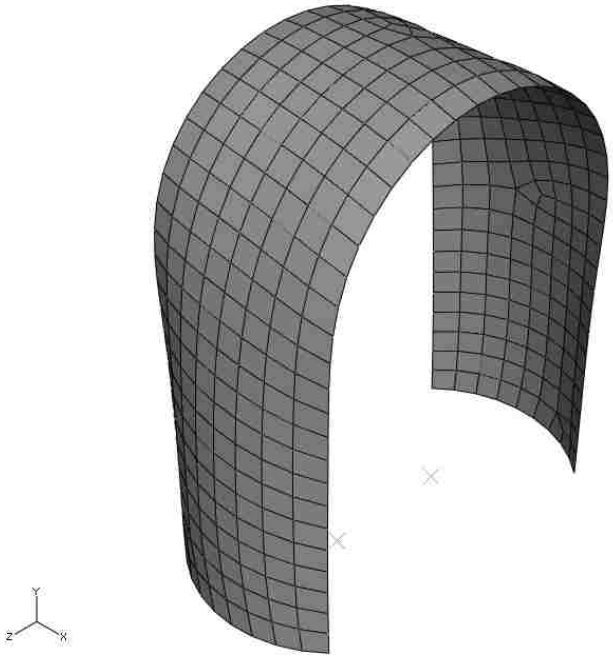

Figure 3. 5: Complete equal-sense folding

To determine the results using these parameters a specified rotation was applied and the reaction moment at the reference point was obtained. A moment-rotation graph could be created by specifying rotations in increments that ranged from 0 to 180 degrees and gathering the respective reaction moments. This was done in increments of five degrees per reference point as shown by Table 4. The first column is the applied rotation in degrees. It only goes to 90 degrees because it is the rotation of one of the two reference points. Column two is the conversion from degrees to radians because Abaqus™ uses radians. The third column is the total rotation of the tape spring and the last column is the resulting moment due to the rotation. This was only analyzed for opposite-sense bending.

Table 4: Results of opposite-sense bending

θ (deg)	θ (rad)	ϕ (deg)	Moment (N-mm)
0	0.000	0	0.0
5	0.087	10	14.2
10	0.175	20	26.0
15	0.262	30	39.9
20	0.349	40	49.7
25	0.436	50	56.9
30	0.524	60	61.0
35	0.611	70	61.7
40	0.698	80	51.5
45	0.785	90	49.0
50	0.873	100	48.0
55	0.960	110	48.0
60	1.047	120	48.0
65	1.134	130	48.0
70	1.222	140	48.0
75	1.309	150	48.0
80	1.396	160	48.0
85	1.484	170	48.0
90	1.571	180	48.0

Figure 3.6 is the moment-rotation graph of the data from Table 4. The results look to be very reasonable by comparing the trend in Figure 3.6 to the general trend for opposite-sense bending in Figure 1.9. This proves that the model and its parameters are correct, and additional analyses with this model should give accurate results.

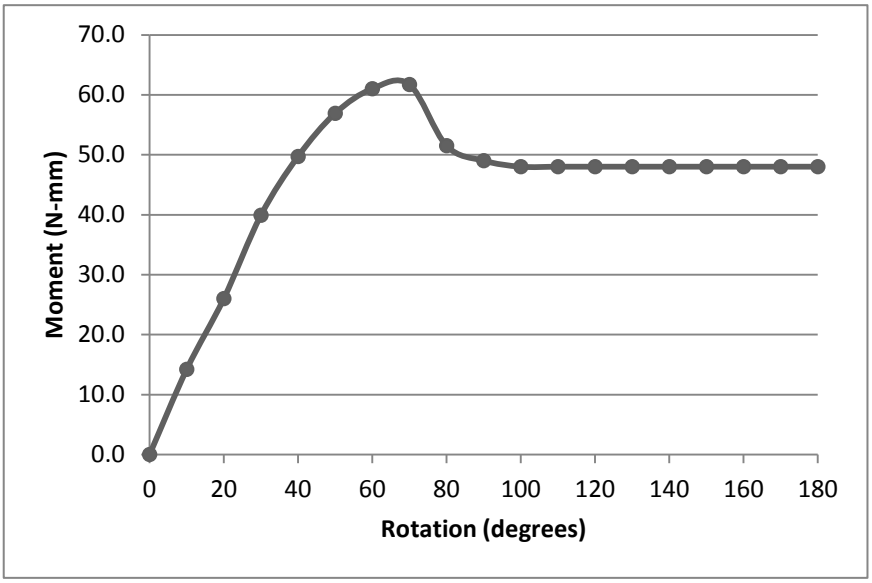

Figure 3. 6: Moment-rotation plot for opposite-sense bending

3.4 Reducing the Peak Moment by Flattening the Middle Section

Tape springs have a higher moment of inertia because of their curved cross section than that of a strip of material that has a flat cross section of the same width and thickness. This higher moment of inertia makes it more difficult to bend the tape spring, which is both a positive and a negative property for the application of a hinge. The high moment of inertia creates a stiffer member when it is in the straight position, which is desired once the structure is in its deployed configuration. The negative aspect of the

higher moment of inertia is the higher moment required to fold the tape spring when trying to reduce the structures size for packing purposes.

Figure 3.6 is a good example of what takes place during the folding of a tape spring. In order for the tape to significantly bend, local buckling must take place. As the moments increase on both ends of the tape, the cross section at the middle of the tape begins to transition from a curved cross section to a flat cross section. Once the cross section becomes flat the tape has a lower moment of inertia and the tape buckles under the increasing moment. In Figure 3.6, flattening of the cross section takes place right at the peak of the trend line. After the peak, or flattening of the cross section creating local bucking, a lower moment is required to either continue to fold the tape farther or to hold the tape at that angle.

In an attempt to reduce the peak that is observed in Figure 3.6, the idea investigated in these analyses was to flatten the middle section of the tape spring before applying the end moments, thus reducing the amount of energy needed to fold the tape spring hinge. Before local buckling normally takes place, all of the energy applied to the tape spring is being used to flatten the cross section of the tape spring. If the cross section is flattened prior to folding, a lower peak moment should result.

This new approach required the creation of an additional step to the tape spring model. The model was broken up into three pieces, two end pieces and a middle section that would be flattened. The analysis would run in two steps just as the plate folding model was a two step process. The first step would be the flattening of the middle section of the tape spring followed by the second step of applying the rotation to the ends of the tape spring.

To create the first step the size (length) of the middle section to be flattened needed to be determined. Since the tape spring is 140 mm long, a 40 mm middle section was arbitrarily chosen leaving 50 mm ends on either side. The model would now include four reference points. The two previous reference points remained in the model while two new reference points were added on each side of the middle of the tape. The 'tie nodes rigid' constraints were also added to the sides of the middle section to help flatten the middle section using the new reference points. These features can be seen in Figure 3.7.

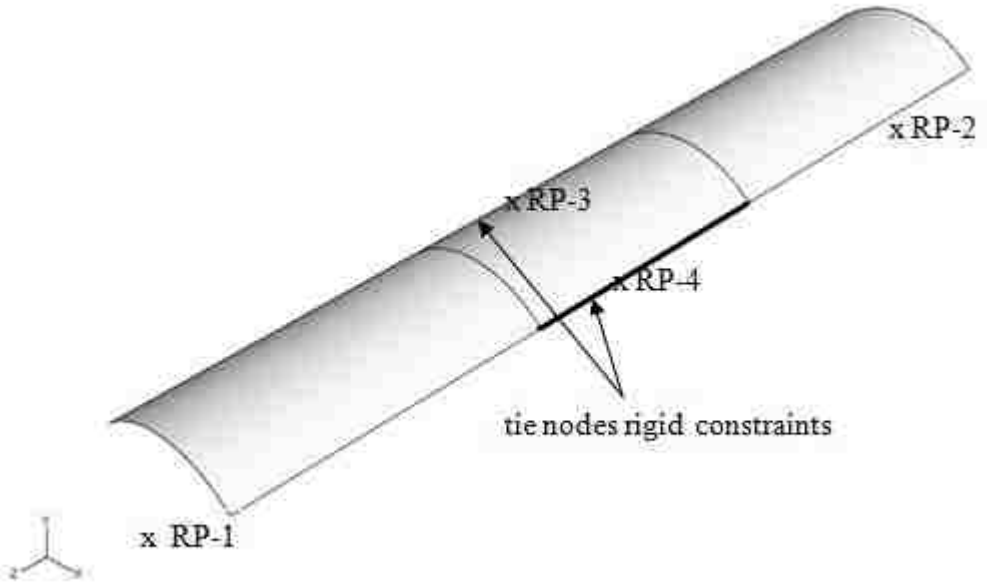

Figure 3. 7: New reference points and constraints

Step one included associating reference points three and four with the new 'tie nodes rigid' constraints. Then as previously described, boundary conditions were added to the reference points to apply a specified rotation that would flatten the middle section. Reference point three was set to have zero displacement in the X-direction, but was free

to move in the Y- and Z-directions. The rotations about the X- and Y-axes were set to zero while the Z-component was set to rotate -0.7549 radians about the Z- axis. Reference point four was free to displace in all directions. The rotations about the X- and Y-axes were set to zero and the Z-component was set to rotate 0.7549 radians about the Z- axis. The value of 0.7549 radians is half of the angle, α, that specifies the tape spring's curvature. This rotation flattened the cross section for the middle segment of the tape as shown in Figure 3.8. Step one was then held while step two was applied to fold the tape spring.

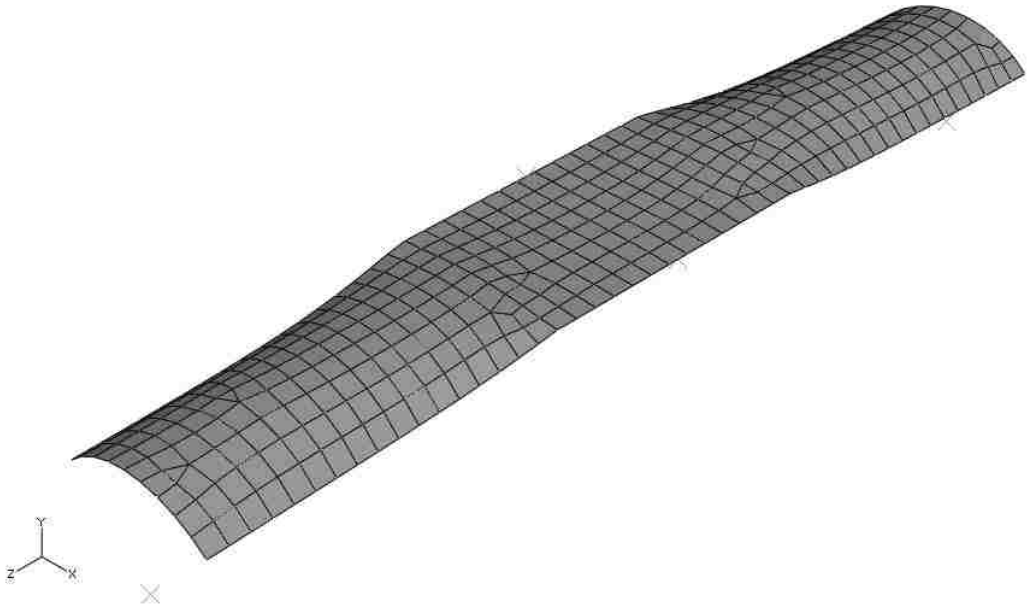

Figure 3. 8: Flattened middle section before step 2 begins

This new method was applied to the model. The first step was run to flatten the middle portion of the tape and hold it flat. The second step folded the tape spring in the opposite-sense direction. The process of collecting the data was the same so that a moment-rotation graph could be produced to compare to Figure 3.6. The reaction moment of flattening the middle section was also obtained to see how much force was

required to flatten it. Below are the results corresponding to the flattened 40 mm middle section.

Table 5: Results of opposite-sense bending after flattening 40 mm middle section

θ (deg)	θ (rad)	ϕ (deg)	Moment (N-mm)
0	0.000	0	0.0
5	0.087	10	4.5
10	0.175	20	15.6
15	0.262	30	24.4
20	0.349	40	31.6
25	0.436	50	37.4
30	0.524	60	41.9
35	0.611	70	45.2
40	0.698	80	47.5
45	0.785	90	48.9
50	0.873	100	49.5
55	0.960	110	49.5
60	1.047	120	49.1
65	1.134	130	48.0
70	1.222	140	47.5
75	1.309	150	47.0
80	1.396	160	47.0
85	1.484	170	47.0
90	1.571	180	47.0

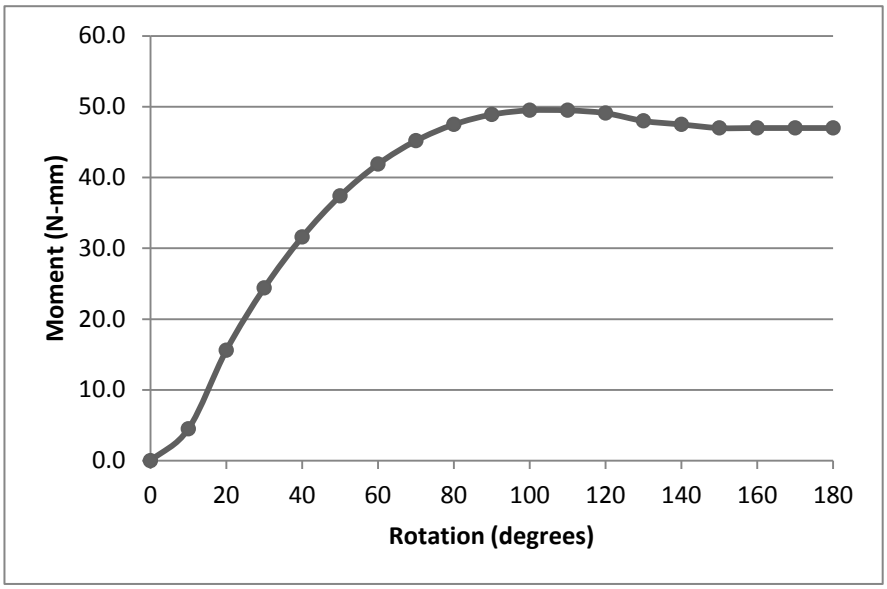

Figure 3. 9: Moment-rotation plot for opposite-sense bending of 40 mm flattened middle section

The results from Figure 3.9 appear to have reduced the peak and flatten the hump in the trend line seen in Figure 3.6 which did not involve flattening of the mid-section. The peak moment from Table 4, normal bending, was 61.7 N-mm. Comparing the peak moment from Table 5, flattening a 40 mm middle section before applying rotation, the peak moment was 49.5 N-mm. This shows that by first flattening the middle section of the tape spring the peak moment needed to fold the tape spring could be reduced.

The other value that the analysis provided was the moment required to flatten the middle section. For a 40 mm middle section, the required moment to flatten the section was 92.3 N-mm. While the peak moment could be reduced by first flattening the middle section, it required a larger moment to flatten the section than to bend the tape spring without first flattening it.

To varify that the flattening moment was the correct value, a moment-curvature equation was applied to check the flattening moment. The equation used was a beam curvature equation, shown in Equation 8.

$$Curvature = \frac{M}{EI} \qquad \textbf{(Eqn. 8)}$$

Where,

Curvature = 1/R, mm
M = moment, N-mm
E = modulus of elasticity, Pa
I = moment of inertia, mm^4

Solving for I,

$$I = \frac{bh^3}{12} = \frac{40mm * 0.115mm^3}{12} = 0.00506mm^4 \qquad \textbf{(Eqn. 9)}$$

Rearranging Equation 8 and solving for M,

$$M = \frac{1}{R} * EI \qquad \textbf{(Eqn. 10)}$$

$$M = \frac{1}{16.91mm} * (2.1x10^5\ N/mm^2 * 0.00506mm^4) = 62.9Nmm \qquad \textbf{(Eqn. 11)}$$

The calculated moment turned out to be 62.9 N-mm, which is lower than the 92.3 N-mm that Abaqus™ calculated. This discrepancy is due to the fact that the equation only looks at a 40 mm segment and ignores the ends that are attached to the rest of the tape spring, a portion of which is also partially flattened in the FEM analyses. The ends would increase the value of the moment as they would add some resistance to the middle

part of the tape as it was being flattened. The numbers are reasonably close, giving confidence that the Abaqus™ 'moment' output is accurate.

Additional analyses were conducted to see what would happen if the length of the middle section was reduced. Flattening the middle section by 40 mm before trying to fold the tape spring lowered the peak moment, but it took a higher moment to flatten the section. Flattening of smaller middle sections 30 mm, 20 mm, and 10 mm were conducted, while keeping a total length of 140 mm. Results are presented and discussed next.

Table 6: Results of opposite-sense bending after flattening 30 mm middle section

θ (deg)	θ (rad)	ϕ (deg)	Moment (N-mm)
0	0.000	0	0.0
5	0.087	10	5.0
10	0.175	20	15.2
15	0.262	30	23.4
20	0.349	40	30.2
25	0.436	50	35.8
30	0.524	60	40.4
35	0.611	70	43.8
40	0.698	80	46.2
45	0.785	90	47.7
50	0.873	100	48.5
55	0.960	110	48.7
60	1.047	120	48.5
65	1.134	130	48.5
70	1.222	140	47.0
75	1.309	150	47.0
80	1.396	160	46.5
85	1.484	170	46.5
90	1.571	180	46.5

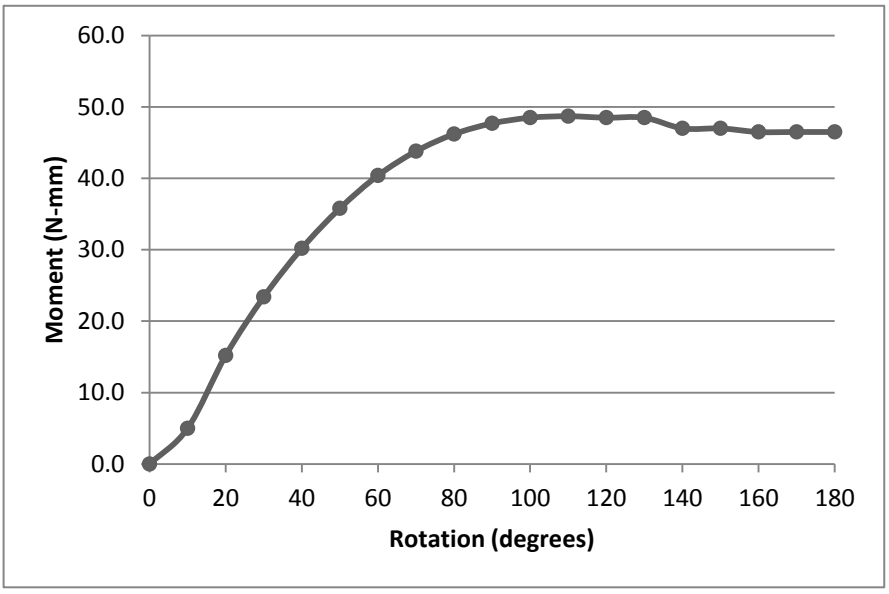

Figure 3. 10: Moment-rotation plot for opposite-sense bending of 30 mm flattened middle section

Reducing the length of the middle section showed to have a better result. The peak end moment was lowered from 49.5 N-mm from the 40 mm middle section to 48.7 N-mm with the 30 mm middle section. The hump in the graph also flattened a little more in Figure 3.10 than the hump of Figure 3.9. The moment required to flatten the middle portion of the tape was also reduced to 77.5 N-mm for the 30 mm middle section. This moment is still higher than the intial peak moment to fold the tape spring, 61.7 N-mm, but as the length of the middle section was reduced the moment to flatten that section was also reduced. By shortening the middle section from 40 mm to 30 mm the flattening moment was reduced by 16%. Reducing the size of the middle section was continued to see if this trend would continue.

Table 7: Results of opposite-sense bending after flattening 20 mm middle section

θ (deg)	θ (rad)	ϕ (deg)	Moment (N-mm)
0	0.000	0	0.0
5	0.087	10	6.1
10	0.175	20	15.4
15	0.262	30	22.6
20	0.349	40	28.6
25	0.436	50	33.8
30	0.524	60	38.3
35	0.611	70	41.9
40	0.698	80	44.8
45	0.785	90	46.8
50	0.873	100	48.1
55	0.960	110	48.6
60	1.047	120	48.7
65	1.134	130	48.5
70	1.222	140	48.0
75	1.309	150	47.5
80	1.396	160	47.3
85	1.484	170	47.0
90	1.571	180	47.0

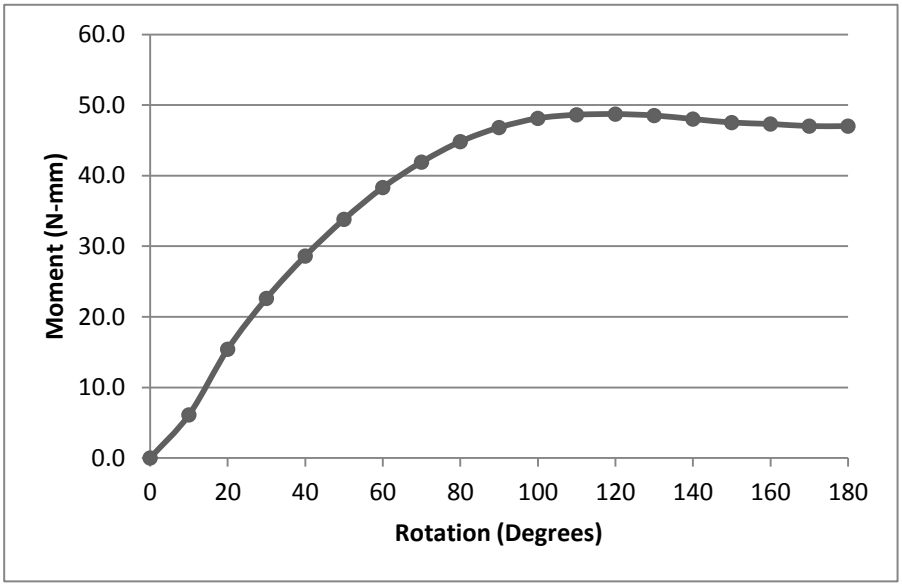

Figure 3. 11: Moment-rotation plot for opposite-sense bending of 20 mm flattened middle section

Table 8: Results of opposite-sense bending after flattening 10 mm middle section

θ (deg)	θ (rad)	ϕ (deg)	Moment (N-mm)
0	0.000	0	0.0
5	0.087	10	10.1
10	0.175	20	19.6
15	0.262	30	26.1
20	0.349	40	30.6
25	0.436	50	34.0
30	0.524	60	37.0
35	0.611	70	39.8
40	0.698	80	42.4
45	0.785	90	44.6
50	0.873	100	46.3
55	0.960	110	47.6
60	1.047	120	48.3
65	1.134	130	48.5
70	1.222	140	48.3
75	1.309	150	48.0
80	1.396	160	47.5
85	1.484	170	47.3
90	1.571	180	47.0

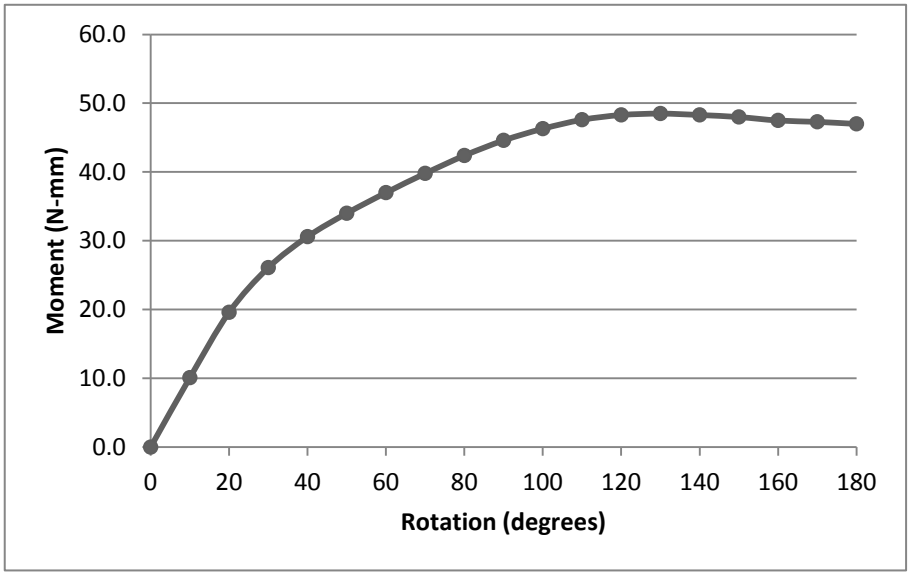

Figure 3. 12: Moment-rotation plot for opposite-sense bending of 10 mm flattened middle section

The results from Tables 7 and 8 along with Figures 3.11 and 3.12 show that the trend continued. As the middle section contiuned to get smaller, the peak in the graphs were lowered and the hump turned into more of a curve. For the 20 mm middle section, the flattening moment was reduced again to 59.1 N-mm. This flattening moment was now lower than the moment of 61.7 N-mm, which was the peak moment of the tape spring without flattening the middle section.

When the middle section was 10 mm long, the flattening moment was reduced to 41.4 N-mm. This moment is now much lower than the moment required to bend the tape spring without a flattened middle section. The 41.4 N-mm flattening moment is also less than the peak folding moment, 48.5 N-mm, to bend the tape spring with a 10 mm middle section. With the middle section small enough, the flattening moment is no longer the governing moment. When the flattening moment was plotted against the middle section length, in Figure 3.13, the result is nearly linear.

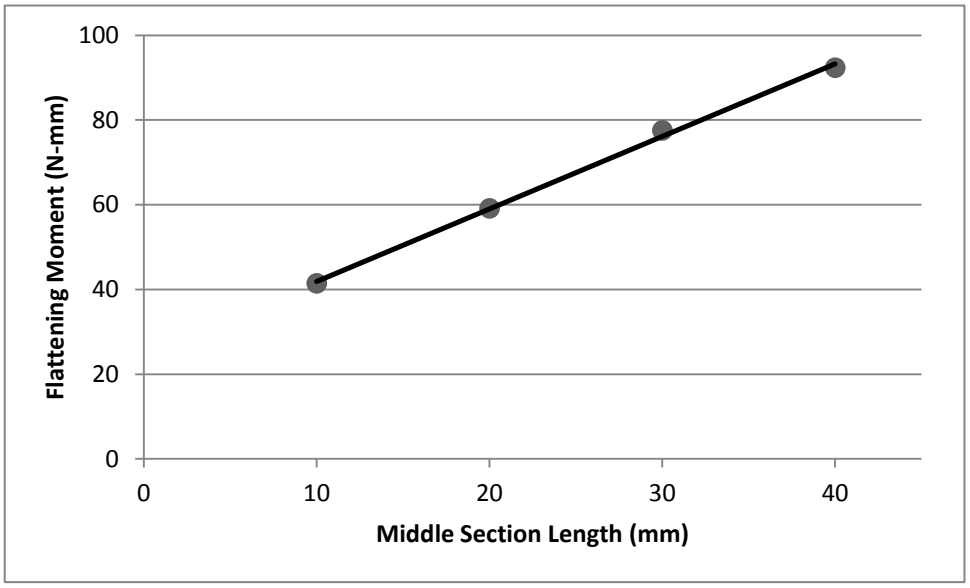

Figure 3. 13: Flattening moment as a function of section length

The results of this tape spring study show an interesting outcome. By flattening the middle cross section of the tape spring before applying the folding moments, the magnitude of the required folding moment can be decreased. However, if the length of the middle section that is flattened is too long, an even greater moment than the peak folding moment is required to flatten the tape spring. By flattening a small length of the cross section, the peak moment can be reduced making it easier to fold the hinge. In this example the peak moment went from 61.7 N-mm down to 48.5 N-mm. This reduced the amount of applied moment by 21% to completely fold the hinge in the opposite-sense direction.

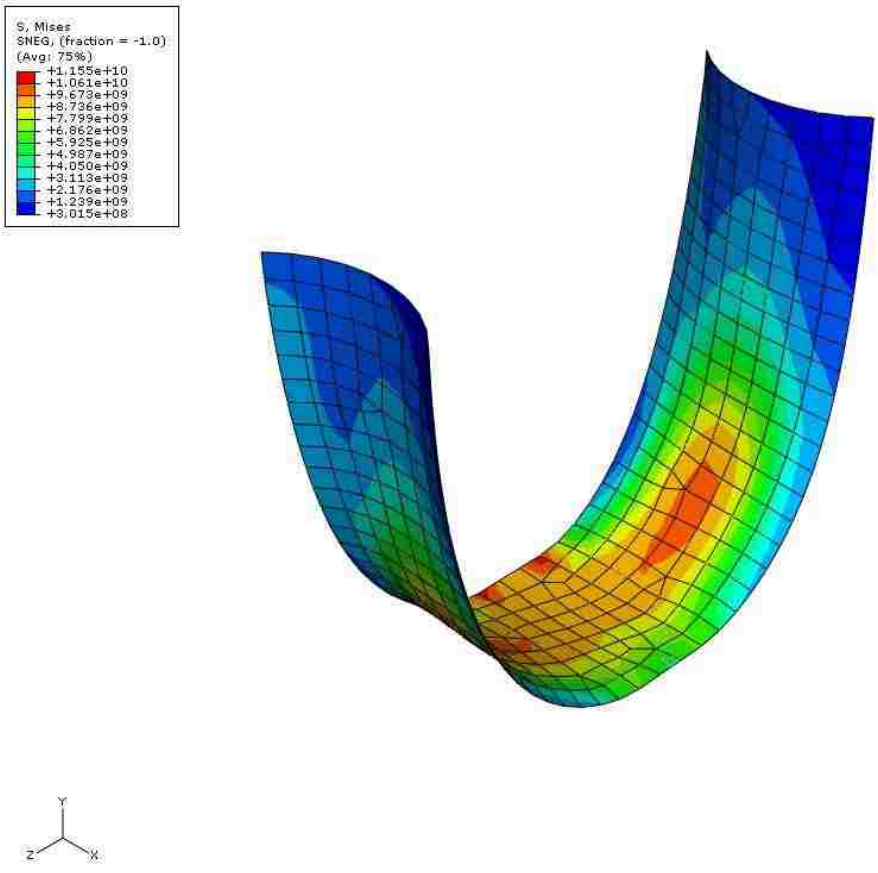

Figure 3. 14: Stresses in the 10 mm tape spring when folded 180 degrees

3.5 Analysis of the Tape Spring Unfolding About the X-Axis

The tape spring hinge was further analyzed by looking at the unfolding characteristics. The same moment-curvature graph was developed for the case of unfolding. As the tape spring is unfolded from the full 180 degrees back to its initial configuration, the cross section of the tape spring goes through a transition. When the tape spring was folded a portion of the middle section of the tape spring was flattened before folding. When the tape spring is released and allowed to unfold, the stored moment allows the two ends of the tape spring to unfold. During the unfolding process, the cross section of the tape spring goes from being flat (Figure 3.15) to its initial curved shape (Figure 3.16). The analysis focused on the effect on the moment-curvature graph as the tape spring was unfolded back to its original shape.

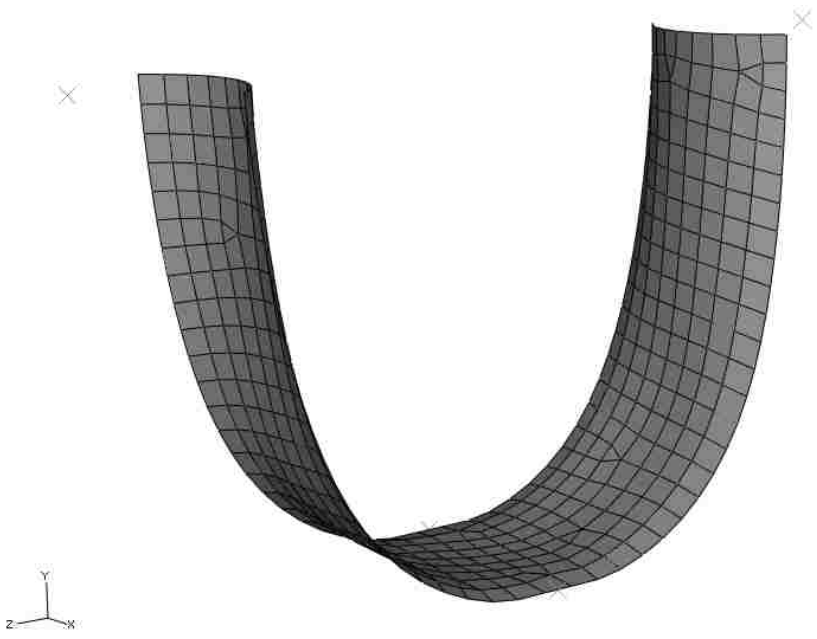

Figure 3. 15: 10 mm middle section is flat at 180 degerees of bending

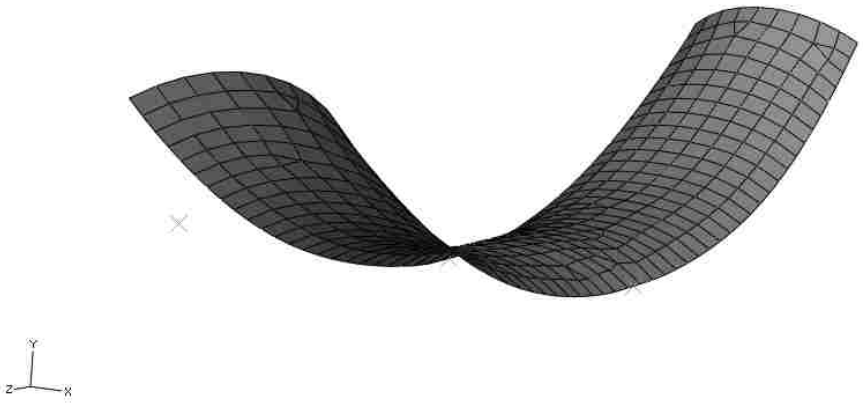

Figure 3. 16: 10 mm middle section regaining its curvature durning unfolding

The analysis procedure was the same as previously described for the folding of the tape spring hinge with the addition of one step to the analysis. The analysis was now a three step process. The first step flattened a specified length of the cross section and held it flat. The second step folded the tape spring from 0 to 180 degrees while the middle section was held flat. The new third step now allowed the tape spring to unfold from 180 to 0 degrees. To make the third step run properly, the first and second steps were inactivated during the unfolding step. Removing the flattening boundary condition allowed the middle cross section to transition from flat back to its original curvature. The third step was run incrementally and the reaction moments were obtained to create the unfolding moment-curvature graph.

The unfolding analysis was only run for the 10 and 20 mm middle sections because these had been shown to be the most efficient ways of flattening the middle section. The other two tests, 30 and 40 mm middle sections, showed that the moment required to flatten the middle section was greater than the moment to fold the tape spring without flattening the middle section.

Table 9: Results of unfolding the 20 mm middle section

ϕ (deg)	Moment (N-mm)
180	50.0
170	49.6
160	49.3
150	49.0
140	48.9
130	49.0
120	49.7
110	51.1
100	53.9
90	58.6
80	63.6
70	66.4
60	66.0
50	62.5
40	54.9
30	44.0
20	31.0
10	16.0
0	0.0

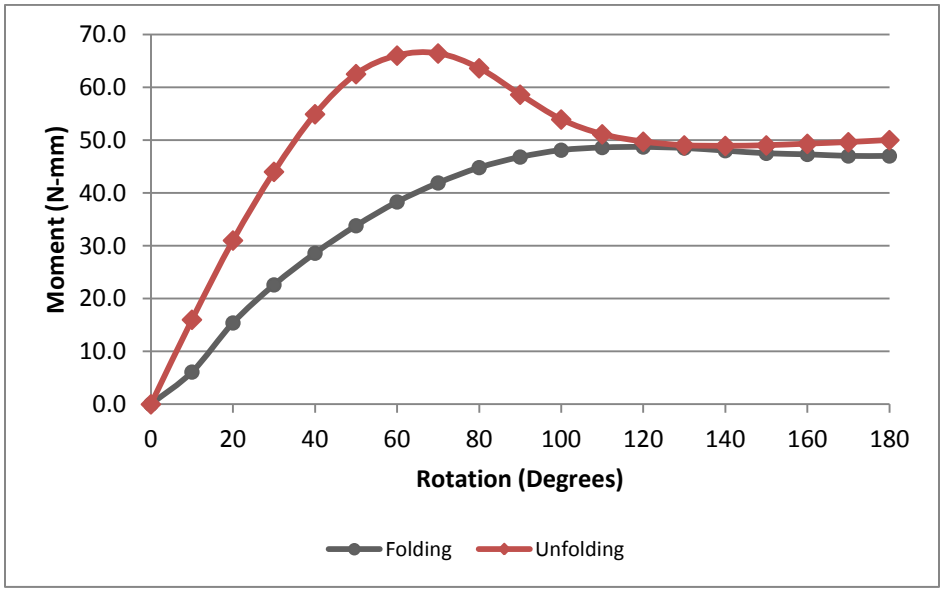

Figure 3. 17: Moment-curvature graph for folding and unfolding the 20 mm middle section

Figure 3.17 shows the behavior of the tape spring as it is folded (lower curve) and then unfolded (upper curve). By flattening the middle section before folding the tape spring, the peak moment is reduced and a flat looking curve is observed. When the tape spring is allowed to unfold and the middle section is also allowed to return to its natural shape a greater moment can be seen. The middle section returning to its natural curviture increases the moment during unfolding.

Table 10: Results of unfolding the 10 mm middle section

ϕ (deg)	Moment (N-mm)
180	48.0
170	48.1
160	48.2
150	48.3
140	48.4
130	48.5
120	48.6
110	48.7
100	49.0
90	50.0
80	61.6
70	64.0
60	63.0
50	59.0
40	52.0
30	42.0
20	29.0
10	15.0
0	0.0

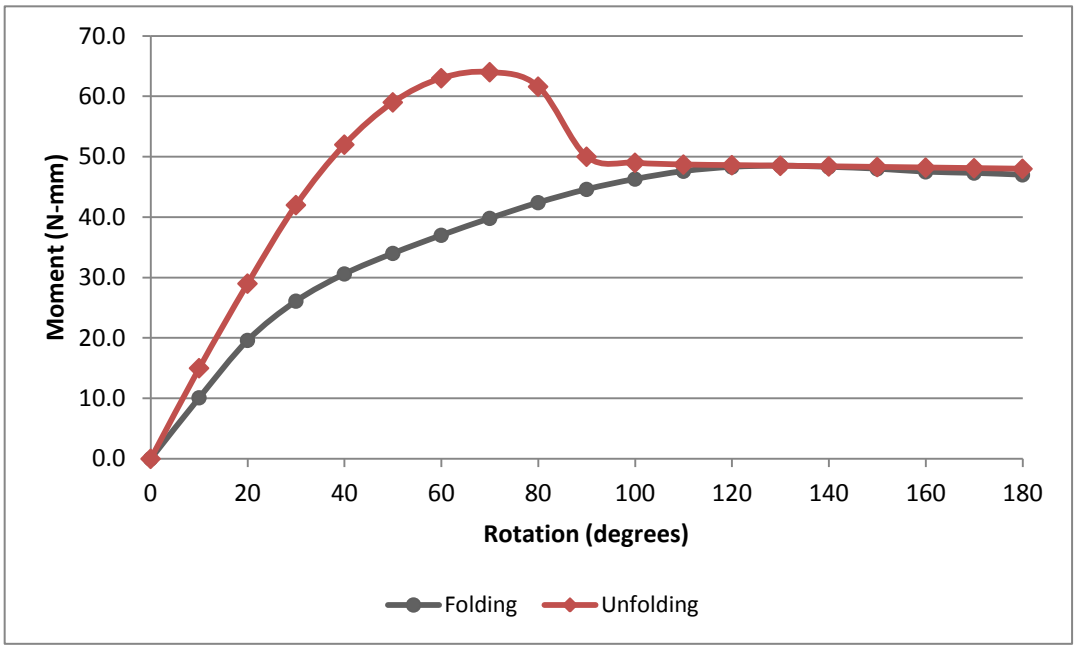

Figure 3. 18: Moment-curvature graph for folding and unfolding the 10 mm middle section

An important outcome is the sustained moment at complete folding. The tape spring required 48.0 N-mm to hold the tape spring at 180 degrees of bending in the case where the middle section was not flattened before bending. This is an important value, because in order to deploy the structure attached to the tape spring hinge, the hinge must have some stored internal moment. When the middle of the tape spring was flattened, the moment at full bending was only slightly lowered. In the case of the 10 mm middle section, the moment at the 180 degree bend was only reduced by 1.0 N-mm to 47.0 N-mm. The stored deployment moment was not affected by flattening the cross section

3.6 Calculating the Energy of the System

Folding the tape spring requires energy and that energy is stored in the tape spring until the tape spring is released. The energy is simply the area under the curve in the

graphs. The amount of energy to fold the hinge and the energy released during unfolding was calculated for both figures. Trapezoidal integration was used to calculate the areas under the curves. The unfolding curve has a greater area in both cases which means that more energy is released in the unfolding of the tape spring than the energy required to fold the tape spring. This difference is due to the fact that the cross section of the tape spring is returning to its natural curvature producing a greater unfolding moment.

Table 11: Energy calculations for the 20 mm middle section

ϕ (deg)	Moment (N-mm)	Unfolding (N-mm)	Area Under Folding	Area Under Unfolding
0	0.0	0.0	30.5	80.0
10	6.1	16.0	107.5	235.0
20	15.4	31.0	190.0	375.0
30	22.6	44.0	256.0	494.5
40	28.6	54.9	312.0	587.0
50	33.8	62.5	360.5	642.5
60	38.3	66.0	401.0	662.0
70	41.9	66.4	433.5	650.0
80	44.8	63.6	458.0	611.0
90	46.8	58.6	474.5	562.5
100	48.1	53.9	483.5	525.0
110	48.6	51.1	486.5	504.0
120	48.7	49.7	486.0	493.5
130	48.5	49.0	482.5	489.5
140	48.0	48.9	477.5	489.5
150	47.5	49.0	474.0	491.5
160	47.3	49.3	471.5	494.5
170	47.0	49.6	470.0	498.0
180	47.0	50.0		
		SUM =	6855.0	8885.0
		Difference	2030.0	
		Energy =	0.354	N-m

Table 12: Energy calculations for the 10 mm middle section

ϕ (deg)	Moment (N-mm)	Unfolding X (N-mm)	Area Under Folding	Area Under Unfolding
0	0.0	0.0	50.5	75.0
10	10.1	15.0	148.5	220.0
20	19.6	29.0	228.5	355.0
30	26.1	42.0	283.5	470.0
40	30.6	52.0	323.0	555.0
50	34.0	59.0	355.0	610.0
60	37.0	63.0	384.0	635.0
70	39.8	64.0	411.0	628.0
80	42.4	61.6	435.0	558.0
90	44.6	50.0	454.5	495.0
100	46.3	49.0	469.5	488.5
110	47.6	48.7	479.5	486.5
120	48.3	48.6	484.0	485.5
130	48.5	48.5	484.0	484.5
140	48.3	48.4	481.5	483.5
150	48.0	48.3	477.5	482.5
160	47.5	48.2	474.0	481.5
170	47.3	48.1	471.5	480.5
180	47.0	48.0		
		SUM =	6895.0	8474.0
		Difference	1579.0	
		Energy =	0.276	N-m

Tables 11 and 12 show the incremental area of each trapezoid in ten degree segments for both the folding and unfolding curves. The sums of the folding and unfolding columns give the total area under each respective curve.

It may appear that when the tape spring unfolded it released a larger amount of energy than the amount of energy that was used to fold the hinge. This is because during the unfolding step, two actions are taking place; the tape spring is unfolding about the short axis while the cross section of the tape spring is returning to its original curvature

about the long axis. This extra energy contribution comes from the flattened cross section releasing its stored energy to the system as the tape spring unfolds.

To satisfy the basic law of conservation of energy there should be no difference in the amount of input energy and the amount of energy released by the system. To verify the total input energy matches the total energy released, the energy to flatten the middle section of the tape spring must also be calculated. The energy to flatten the middle section should be equal to the energy difference between the folding and unfolding of the tape spring. The analysis was done by incrementally flattening the cross section and obtaining the reaction moment resulting from the applied rotation.

Table 13: Engergy calculations for flattening the 20 mm middle section

θ (deg)	Moment Z (N-mm)	Area Under Flattening	
0	0.0	17.5	
5	7.0	53.0	
10	14.2	88.3	
15	21.1	122.8	
20	28.0	179.8	
25	43.9	213.8	
30	41.6	224.5	
35	48.2	257.3	
40	54.7	186.1	
43.27	59.1		
	SUM =	1342.8	
	Energy =	0.234	N-m

Table 14: Energy calculations for flattening the 10 mm middle section

θ (deg)	Moment Z (N-mm)	Area Under Flattening	
0	0.0	12.0	
5	4.8	36.3	
10	9.7	60.5	
15	14.5	84.3	
20	19.2	108.0	
25	24.0	132.0	
30	28.8	155.8	
35	33.5	179.5	
40	38.3	130.3	
43.27	41.4		
	SUM =	898.6	
	Energy =	0.157	N-m

Tables 13 and 14 show the calculation for the energy required to flatten the middle section. 'Sum' is the total area under the moment-curvature graph in units of N-mm-degrees. 'Energy' is the unit conversion from N-mm-degrees to N-m-radians. These energy values from Tables 11 through 14 were evaluated using Equation 12 to investigate the energy balance for the system. Flattening and folding involve energy inputs (stored strain energy) into the tape spring while unfolding results in the release of energy. The release of energy is in the form of kinetic energy which needs to be damped out. The energy stored or released during the 3 separate steps should satisfy the conservation of energy principle as depicted in Eqn. 12:

$$Flattening + Folding - Unfolding = 0 \qquad \textbf{(Eqn. 12)}$$

For the 20 mm middle section,

$$1343 + 6855 - 8885 = -687 \text{ N-mm-degrees} \qquad \textbf{(Eqn.13)}$$

For the 10 mm middle section,

$$899 + 6895 - 8474 = -680 \text{ N-mm-degrees} \qquad \textbf{(Eqn.14)}$$

It can be seen that while energy is conserved to within 8% of the total (difference in Eqn. 13 and 14 are less than 8% of the energy stored or released), there is some unexplained stored energy (687.2 and 680.4 N-mm in Eqns. 13 and 14), This discrepancy is due to the following. During the initial flattening, nodes on the side of the flattened section are constrained in displacement. This constraint is later removed after the tape-spring has been folded resulting in a small adjustment of the internal energy state (notice the small jump at the right end of Figures 3.17 and 3.18). Additional displacement caused by the release of these boundary conditions result in some additional strain energy that could not be captured in this analysis. The artificial damping used in the analysis also contributes to the energy difference.

3.7 Conclusion

A nonlinear finite element analysis was conducted to evaluate the complete 180 degree folding and unfolding of a curved tape spring. The analysis can be used for complex geometries, for any elastic material (such as composites) and can also be extended to inelastic materials.

This study of tape springs and the mechanics of folding tape springs showed that flattening a small portion of the cross section at the middle of the tape spring can reduce the peak moment of folding the tape spring. This can help reduce the cost and weight of actuators needed for stowage and deployment. By flattening the cross section, the

moment of inertia was reduced making it easier to fold the tape spring about the short axis.

It is known that in the absence of inelastic behavior (damage or plastic deformation), energy put into the system will be stored and subsequently released by the system. While the peak folding moment about the short axis was reduced, and the energy to fold the tape spring about the short axis was also reduced. During the unfolding process, the applied energy of the system is released as the tape spring unfolds while simultaneously regaining its initial curved cross section. The energy released is important for determining the dynamics of the structural system and designing adequate damping methods. Damping of the extra energy is important to avoid the possibility of the overshoot effect, osculating, and vibration in the structure.

Ability to analytically determine the moment-curvature and energy release is important for designing space-based sensor structures that are very fragile or have very sensitive equipment attached.

References

Aglietti, S. J. (2007). A study of tape spring fold curvature for space deployable structures. *Journal of Areospace Engineering* , 313-325.

Beavers, F. L., Munshi, N. A., Lake, M. s., Maji, A., Qassim, K., Carpenter, B. F., et al. (2002). Design and Testing od an Elastic Memory Composite Deployment Hinge for Spacecraft. *43rd Structures, Structural Dynamics, and Materials Conference* (pp. 1-5). Denver: American Institue of Aeronautics and Astronautics.

Daily, D. I. (2011, May 25). *NPOESS Weather Satellites: From Crisis to Program Splits*. Retrieved August 19, 2011, from Defense Industry Daily: http://www.defenseindustrydaily.com/major-shifts-flow-from-npoess-polar-satellite-program-crisis-01557/

Dassault Systemes Simulia Corp. (2010). *Introduction to Abaqus V. 6.10.*

Dassault Systems Simulia Corp. (2009). Abaqus/CAE Version 6.9. Providence, RI, US.

Gantes, C. (2001). *Deployable Structures: Analysis and Design.* Boston: WIT Press.

Hibbeler, R. C. (2008). *Mechanics of Materials Seventh Edition.* New Jersey: Pearson Prentice Hall.

Hibbeler, R. C. (2006). *Structural Analysis Sixth Edition.* New Jersey: Pearson Prentice Hall.

Hoffait, S., Bruls, O., Granville, D., Cugnon, F., & Kerschen, G. (2010). Dynamic Analysis of the Self-locking Phenomenon in Tape-Spring Hinges. *Acta Astronautica* , 1125-1132.

J.C.H. Yee, O. S. (2004). Carbon Fibre Reinforced Plastic Tape Springs. *Ameican Institute of Aeronautics and Astronautics*, (pp. 1-9). Palm Springs, California.

Kiper, G., & Soylemez, E. (2009). *Deployable Space Structures.* IEEE.

Neogi, D., Douglas, C., & Smith, D. R. (1998). Experimental Development of Self-deployable Structures. *International Journal of Space Stuctures* , 157-158.

Ng, T.-T. (2006). Numerical Simulations of a Deployable Structure. *Earth and Space* .

Seffen, K., Pellegrino, S., & Parks, G. (2000). Deployment of a Panel by Tape Spring Hinges. *IUTAM-IASS Symposium on Deployable Structures: Theory and Applications* (pp. 355-364). Kluwer Academic Publishers.

Soykasap, O. (2007). Analysis of Tape Spring Hinges. *International Journal of Mechanical Sciences, Vol. 49, Issue 7* , 853-860.

Walker, S. J., & Aglietti, G. S. (2007). A Study of Tape Spring Fold Curvature for Space Deployable Structures. *Journal of Aerospace Engineering* , 313-325.

Yee, J., & Pellegrino, S. (2005). Composite Tube Hinges. *Journal of Areospace Engineering* , 224-231.

Zhang, P. (Performer). (2010, August 2-6). *Introduction to Abaqus Training Course.* Woodbury, Minnesota, U.S.